APPLICATION OF VEHICLE-BASED SENSORS ASSESSING HIGHWAY PAVEMENT CONDITIONS SUBJECT TO EXTREME TEMPERATURE VARIATION

By Matthew C. Snyder

A Thesis

Submitted in Partial Fulfillment

Of the Requirements for the Degree of

Master of Science

In Civil Engineering

Northern Arizona University

May 2018

Approved:

Chun-Hsing Ho, Ph.D., P.E., Chair

Edward J. Smaglik, Ph.D., P.E.

Brendan J. Russo, Ph.D.

Abstract
The technique of using vibration sensors to monitor pavement roughness has been expanding in pavement engineering. The primary objective of this study is to implement cost-effective vibration sensors to predict asphalt roughness and identify critical cracking locations. It has been an increasing discussion in industry whether temperature changes due to climate change will have considerable influence on infrastructure resilience and sustainability. The method presented here uses vehicle-based sensors to assess pavement roughness during extreme hot and cold temperatures in Phoenix, AZ. This project consisted of developing vehicle-based accelerometers and taking monthly road surveys for a year. Five sensors were mounted to a vehicle, four on the tires and one inside the car, as well a sixth smartphone sensor inside the car. This project covers collecting data at pavement temperatures from 40ºF - 150ºF. The analysis consists of converting accelerometer data into international roughness index values using Fourier transforms and using statistical analysis to verify a relationship between pavement temperature and accelerometer vibration. The results show that hot asphalt concrete temperatures increase the amount of observable accelerometer vibration from a vehicle. Sensors mounted near the tires showed to be more reliable than sensors inside the vehicle. This project demonstrates that accelerometer sensing technology is a cost-effective way to advance the day-to-day operations in highway pavement maintenance and management.

Acknowledgements

I would like to first thank my advisor Dr. Chun-Hsing Ho for inspiring me to pursue a master's degree. He has been with me my entire NAU career and has opened doors and connections with people in the pavement design and materials science industry I would never have been aware of. I would also like thank the rest of my advisory committee: Dr. Brendan Russo and Dr. Edward Smaglik for involving me within NAU's research project with the Arizona Board of Regents (ABOR) and being supportive when networking in the transportation industry. This project would not have been possible without the programming skills of Zhilian He when developing the graphical user interface necessary for data collection. I would like to thank Bilal Habib and Raul Chipana Quispe from NAU's School of Informatics, Computing, and Cyber Systems for allowing me to use their soldering equipment and expertise. The facility at NAU's fleet services provided tremendous support for allowing us to rent the same vehicle every month and install our sensors to it. Many thanks to my peers Amal Abdelaziz, Brandon Dunn, Samuel Taylor, and Max Burke for being by my side as I presented and conducted road tests. Lastly, I would like to thank my family for being so supportive and believing in me the entire time.

Table of Contents

Abstract ii

Acknowledgements iii

List of Figures v

1.0 Introduction: 1

1.1 Research Questions 2

2.0 Background 2

3.0 Methodology 7

3.1 System Components 8

3.2 Study Location 14

4.0 Results 15

4.1 Threshold method 16

4.2 Average Method 24

4.3 GIS Mapping 28

5.0 Analysis 39

5.1 Tire Pressure 39

5.2 IRI Conversion 41

5.3 Statistical Significance 45

6.0 Conclusions: 48

6.1 Recommendations 50

References 51

List of Figures

Figure 1: Left: ADOT road profiler. Profiler is the gray box mounted on the front. Right: South Dakota road profiler with lasers sensors mounted on top. [11] 3
Figure 2: Quarter-car model. [15] 4
Figure 3: Half-car Model. [15] 5
Figure 4: Conceptual framework 7
Figure 5: Top: ADXL 335 accelerometer. Bottom: Adafruit GPS. Right: TP-LINK 3G router. 8
Figure 6: All sensors and GPS used in system. 9
Figure 7: Accelerometer placement on vehicle. 10
Figure 8: GUI during road test traveling at 60-mph. 12
Figure 9: GUI during road test traveling at 0-mph. 12
Figure 10: GoPro Hero5 display. 13
Figure 11: Road test site. Phoenix, AZ. 27th Ave. - 51st Ave. and Baseline Rd. - Chandler Blvd. 175
Figure 1: Using the Threshold method on raw data. 17
Figure 13: Threshold method showing how vibration increases with temperature. 18
Figure 14: Threshold method – smartphone sensor does not sense change in temperature. 18
Figure 15: Threshold method over a year. 27th Ave. - 51st Ave. East Bound Lane 1. 20
Figure 16: Threshold method over a year. 27th Ave. - 51st Ave. East Bound Lane 2. 20
Figure 17:Threshold method over a year. 27th Ave. - 51st Ave. West Bound Lane 1. 21
Figure 18: Threshold method over a year. 27th Ave. - 51st Ave. West Bound Lane 2. 21
Figure 19: Threshold method over a year. Baseline Rd. - Chandler Blvd. East Bound Lane 1. 22
Figure 20: Threshold method over a year Baseline Rd. - Chandler Blvd. East Bound Lane 2. 22
Figure 21: Threshold method over a year. Baseline Rd. - Chandler Blvd. West Bound Lane 1. 23
Figure 22: Threshold method over a year. Baseline Rd. - Chandler Blvd. West Bound Lane 2. 23
Figure 23: Average method over a year. 27th Ave. - 51st Ave. East Bound Lane 1. 24
Figure 24: Average method over a year. 27th Ave. - 51st Ave. East Bound Lane 2. 25
Figure 25: Average method over a year. 27th Ave. - 51st Ave. West Bound Lane 1. 25
Figure 26: Average method over a year. 27th Ave. - 51st Ave. West Bound Lane 2. 26
Figure 27: Average method over a year. Baseline Rd. - Chandler Blvd. East Bound Lane 1. 26
Figure 28: Average method over a year. Baseline Rd. - Chandler Blvd. East Bound Lane 2. 27
Figure 29: Average method over a year. Baseline Rd. - Chandler Blvd. West Bound Lane 1. 27
Figure 30: Average method over a year. Baseline Rd. - Chandler Blvd. West Bound Lane 2. 28
Figure 31: 27th Ave. – 51st Ave. Top to bottom: severe and moderate cracks for east and west bound lane 1 in March, June, September, and December. 29
Figure 32: Baseline Rd. – Chandler Blvd. Top to bottom: severe and moderate cracks for east and west bound lane 1 in March, June, September, and December. Figure is broken up into north and south segments for each month to view the detail. 37
Figure 33: ADOT IRI values mapped with individual cracks located from the accelerometers. 38

Figure 34: Threshold method - effects of tire pressure. 40
Figure 35: Average method - effects of tire pressure. 40
Figure 36: Discrete Fourier transform moving through raw data. 43
Figure 37: IRI comparison. 27th Ave. - 51st. Ave. east bound. 43
Figure 38: IRI comparison. 27th Ave. - 51st. Ave. west bound. 44

Figure 39: IRI comparison. Baseline Rd. - Chandler Blvd. east bound. 44
Figure 40: IRI comparison. Baseline Rd. - Chandler Blvd. west bound. 45
Figure 41: ANOVA test. Threshold method. Temperature vs. vibration. 46
Figure 42: ANOVA test. Average method. Temperature vs. vibration 46
Figure 43: T-test IRI comparison. 27th Ave. - 51st. Ave. east bound. 47
Figure 44: T-test IRI comparison. 27th Ave. - 51st. Ave. west bound..... 47
Figure 45: T-test IRI comparison. Baseline Rd. – Chandler Blvd. east bound. 47
Figure 46: T-test IRI comparison. Baseline Rd. – Chandler Blvd. west bound. 47
Figure 47: Sensor M5 inside the vehicle is a linear function of all tires M1-M4. 48

1.0 Introduction:

A roads roughness has important contributions to road-user costs, vehicle delay costs, crash costs, and noise pollution. When a road becomes rougher, the vehicles driving over it will experience increased vibration that contributes to faster deterioration of a pavement structure. These significant consequences have led highway agencies to pay more attention to the roughness levels of their pavements.

Current methods of evaluating road roughness can be costly using sophisticated sensing equipment. When a highway engineer is deciding when/where to commence pavement rehabilitation, it is ideal to know the condition of all nearby roads as to prioritize which rehabilitation should come first. The primary objective of this study is to develop a cost-effective sensing technology that highway agencies can use to quantify pavement roughness while providing locations of critical fatigue cracking and rutting. It is in popular discussion that global warming with contribute to unexpected temperatures over the next decades. This data will assess a range of temperatures and determine whether temperature plays a role in roughness quantification.

The scope of this project contains devising vehicle-based vibration sensors, collecting data based on temperature variations, identifying severe and moderate cracks, converting to a roughness index that highway agencies can use, and predicting pavement behavior under a range of temperatures. Sensors were tested on bicycles to determine the accuracy of the accelerometer sensors. Other concurrent data collection included controlling tire pressure to see the effects of tire pressure on vibration. The same vehicle was used throughout the data

collection process, a 2016 Honda Accord. Tire pressures were recorded each test with a tire pressure gauge and pavement surface temperatures were measured with an infrared thermometer.

1.1 Research Questions

The questions asked throughout this research are:

1. Can accelerometers accurately predict highway pavement roughness conditions?
2. Does pavement temperature have a significant effect on accelerometer sensing?
3. What can accelerometer sensors predict that is different from the current state-of-art method of evaluating pavement conditions?

The broader question is what effect does extreme temperatures have on asphalt?

2.0 Background

The “roughness” level of a pavement network is useful for highway agencies to monitor their pavement health. The first International Road Roughness experiment in 1986 [14] defines “roughness” as the variation in surface elevation that induces vibrations in traversing vehicles. A standardized roughness scale, the International Roughness Index (IRI), was created in 1986 by the World Bank and is used to define a characteristic of the longitudinal profile of a traveled wheel track [13] More precisely, the IRI is a longitudinal measure of how the surface of a pavement deviates over a specified distance, also known as the average rectified slope (ARS) with units of in/mi, m/km, etc... The IRI is a ratio of suspension motion over distance traveled based on a simulation of a car going 50-mph. The higher the IRI value, the higher the roughness level of a road. Besides for routine monitoring, the initial roughness after construction is

measured and is a key factor in providing long-term performance. The smoother a pavement is built, the smoother it stays over time [6].

According to the World Bank [13], there are four common techniques for measuring roughness, listed from most expensive to least expensive: 1) Direct profile measurements using lasers to survey the road while driving. 2) Indirect profile measurements using manual methods of level and rod surveying. 3) Response type road roughness measurement systems (RTRRMSs) using sensors to measure the response of a vehicle driving over a pavement. 4) Subjective rating panels using judges to inspect a road and rate it based on intuition and experience. All techniques can be converted into IRI values. This project uses RTRRMS techniques.

The more common IRI measuring systems used today are installed on vans or trucks and contain microcomputers and data processing instruments which measure differences in ultrasonic or light profiles. For example, a hybridized South Dakota road profiler, Figure 1, combines three ultrasonic sensors with two laser sensors, one for each wheel path, and combines both sensing techniques and resultant IRI calculations [11].

***Figure 2**: Left: ADOT road profiler. Profiler is the gray box mounted on the front. Right: South Dakota road profiler with lasers sensors mounted on top. [15]*

IRI is measured in certain wheel paths. A quarter-car model is used to calculate IRI and is shown in Figure 2. The model summarizes how roughness causes vibrations of the car. It includes tire compliance suspension stiffness and dampening.

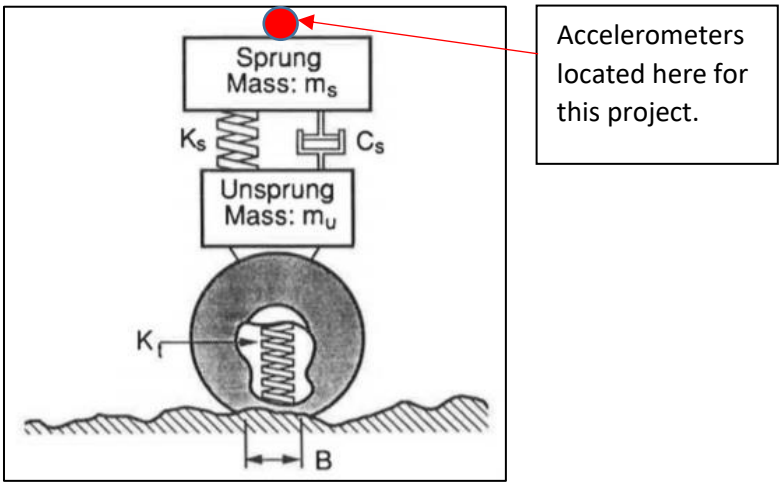

***Figure 3**: Quarter-car model. [15]*

Newton's second law of motion states that the acceleration of an object as produced by a net force is directly proportional to the magnitude of the net force. Therefore, when drawing a free body diagram the following differential equations are obtained [19]:

$$m_s\ddot{Z}_s + C_s(\dot{Z}_s - \dot{Z}_u) + K_s(Z_s - Z_u) = 0$$

$$m_s\ddot{Z}_u + C_s(\dot{Z}_u - \dot{Z}_s) + K_s(Z_u - Z_s) = K_t(Z_p - Z_u)$$

Z_p = the input: wheel track elevation as a function of time.

m_s and m_u = sprung and unsprung masses respectively.

K_s = linear spring stiffness of the suspension system.

C_s = dampening rate of the suspension system.

K_t = linear spring stiffness model of tire.

Z_u= vertical displacement of unsprung mass Z_s= vertical displacement of spring mass

After removing the masses from the equations and solving, the response of the quarter-car model traveling at 50-mph can be calculated for each point, x, along a distance of travel, L.

The IRI is:

$$IRI = \frac{1}{L}\int_0^L |Z_s - Z_u|\, dx$$

The quarter-car model analyzes road conditions for a single wheel track. This study analyzes road conditions using two traveled wheel tracks also known as a half-car model, Figure 3, and therefore calculates a half-car roughness index (HRI). Sayers [15] has shown that the average of the IRIs from the two traveled wheel tracks are always lower than the average of the IRIs from one traveled wheel track and recommends this equation:

$$HRI = 0.8IRI$$

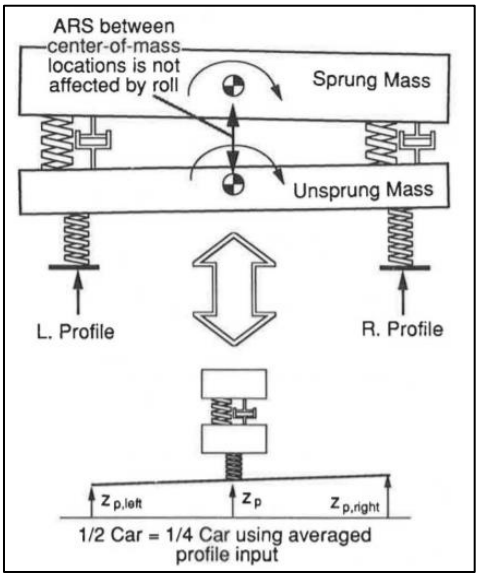

***Figure 4**: Half-car Model. [15]*

Decisions on which type of model to use depends on practical considerations. Sayers [15] warns that there has been confusion between the two methods and data is being reported without specifying which method is being used.

Recent studies [4], [5] have shown that using inexpensive accelerometers can be converted into IRI data. This research project differs from other accelerometer methods by placing accelerometers on each wheel of a vehicle and inside the vehicle to be compared with a smartphone sensor. Also, instead of using only the z-axis responses for IRI conversion, the total magnitude of the x, y, and z directional responses are used.

Smartphone accelerometers has become a growing technique in evaluating pavement roughness using RTRRMS methods. Because of the convenience of smartphones with built-in accelerometers, vibration applications have been a topic of research for advancing pavement monitoring systems. Recent studies [2], [3], [8] showed that acceleration vibration magnitude has a linear relationship with road roughness conditions and IRI values measured by smartphone application are very close to IRI values measured by highway agencies when pavement conditions are “good” to “fair” in terms of roughness.

Studies [10], [12] have shown that Geographic Information Systems (GIS) is useful in combining layers of roadway information to benefit decision-making processes of road intervention. Using a tool like GIS can combine crash hotspots with a roughness index to determine where road intervention should occur. Accelerometers have been paired with GIS platforms and shown effectiveness [8]. Other studies [9] have shown GPS data refinement methods need to be implemented to improve accuracy.

Tire pressure and dampening systems are known to play a key role in how a vehicle responds to a roads roughness. Studies [7], [17] have shown that tire pressure has significant effect on RTRRMSs. Tire size, tire construction, inflation pressure, and operating conditions also influence the vibration experienced by a vehicle.

3.0 Methodology

Vehicle-based accelerometers were developed in lab and used in conjunction with a smartphone accelerometer sensor application. Data is collected while driving at highway speeds and transmitted to a laptop inside the vehicle using a WiFi router with local access. Five accelerometer sensors were mounted to the vehicle, one on each wheel's control arm (M1-M4), one inside cab of the vehicle (M5), and a sixth iPhone sensor mounted inside the cab of the vehicle. The conceptual framework of the system is shown in Figure 4. Accelerometers located by each wheel transmits data wirelessly through a router to an on-board computer. GPS is linked to each accelerometer for data to be georeferenced. Smartphone data and video data are transmitted separately from the accelerometer sensors.

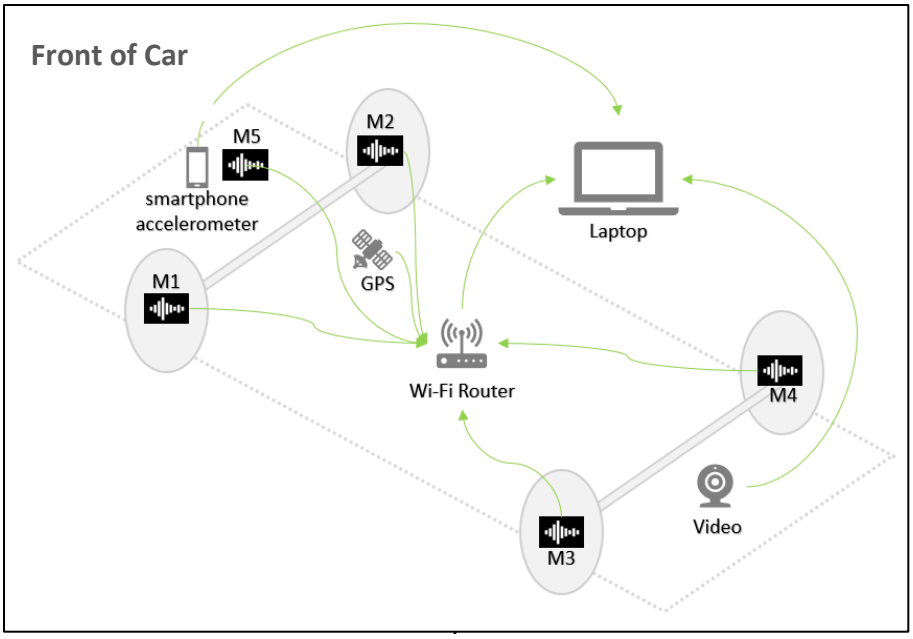

***Figure 5**: Conceptual framework*

3.1 System Components

ADXL 335 triple-axis accelerometers were developed with Arduino MKR1000 computer boards. Components were soldered together in NAU's technology lab. The sensors communicate three-dimensional vibration data to a laptop using WiFi. The sensors are attached to each wheel's control arm using project boxes with Velcro. Velcro is meant to limit the movement of the sensors on the control arm and only catch the movement of the control arm itself. Foam is used inside the project boxes as to limit sensor movement during the ride. The fifth ADXL 335 sensor is located inside the vehicle next to an iPhone sensor, taped to the center console. An Adafruit Ultimate GPS is also connected to an Arduino MKR1000 computer board and used in conjunction with the ADXL 335 accelerometers. The accelerometer, GPS, and WiFi router is shown in Figure 5.

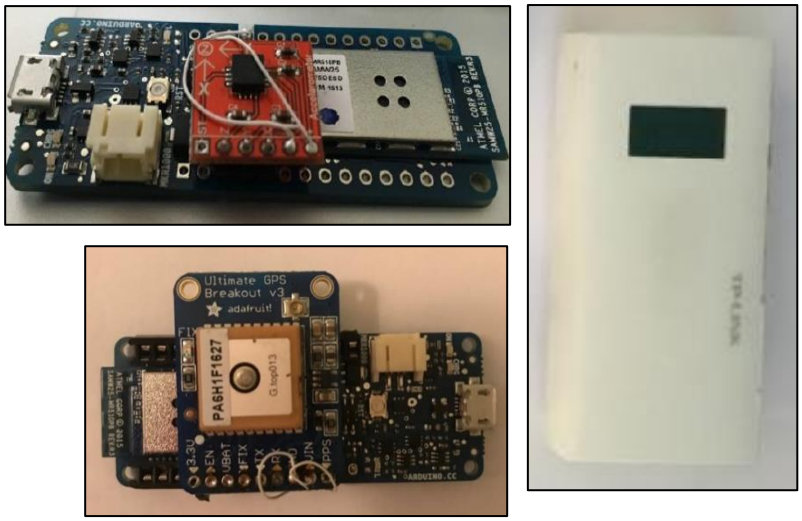

***Figure 6**: Top: ADXL 335 accelerometer. Bottom: Adafruit GPS. Right: TP-LINK 3G router.*

The cost of one unit of the ADXL 335 triple-axis accelerometer, Arduino MKR1000, and Adafruit Ultimate GPS is $10.00, $40.00, and $35.00 respectively. The wireless router that was used was a Unicom 3G router with a cost of $120.00. The project enclosures and foam are roughly $5.00.

Figure 7: *All sensors and GPS used in system.*

All sensors and GPS devices are shown in Figure 6. The team visited the transportation fleet center at NAU to acquire a testing vehicle and discuss where the best placement for the sensors were. A 2016 Honda Accord from NAU's fleet was best suited for the experiment. To determine where to place the sensors, the team discussed ideas with the technicians while the vehicle was lifted in the air. The objective was adequate placement as to catch suspension motion, level surface for sensors to sit, and easy install so this could be done quickly in the field without having to jack up the vehicle. The control arms were chosen as they are responsible for connecting a vehicles suspension to its frame and provide a flat surface to mount sensors.

***Figure 8**: Accelerometer placement on vehicle.*

The sensors had to be able to be removed from the vehicle when the team was not testing. During a field test, the sensors could be mounted in the front by turning the steering wheel all the way to one direction, reaching in, and placing project enclosure on a Velcro sticker. Sensors

were mounted in the back by laying down on the ground and reaching up to the rear control arms. Sensor placement on the testing vehicle is shown in Figure 7.

A graphical user interface (GUI) laptop application was developed to display the real-time data and to store the data in .csv files with a start/stop function. The blue, green, and red colors represent the x, y, and z-axis respectively. There are five displays for the five sensors mounted on the vehicle. The top four displays are for the sensors located on front driver-side tire, front passenger-side tire, back driver-side tire, and back passenger-side tire respectively. The bottom right corner of the GUI is the sensor mounted inside the vehicle. Notice how the overall magnitude of the sensor inside the vehicle is less than the magnitude of the sensors located on the tires due to the vehicles suspension system. The GUI shows latitude, longitude, and speed. It also allows you to view the scatter plots at different speeds and adjust the frequency of how milliseconds per point. After experimenting with the frequency, approximately 30 data points per second are collected during a field test.

Road tests were conducted with two people, the driver and the passenger. The driver is responsible for maintaining a constant test speed while driving safely and smoothly. The passenger of the vehicle is responsible for running the laptop and controlling the GUI, so the driver is not distracted. The passenger oversees starting/stopping data collection, renaming each test run, note keeping of road conditions, and keeping an extra eye on the road to help the driver.

The GUI is shown below. Figure 8 is an example of data collection traveling at 60-mph. Figure 9 is when the vehicle is still. If the sensor was at perfectly level position, the blue, green, and red,

colors would show up on top of each-other. The slight degree of off-level position is due to the control arms not being completely flat and the accelerometers not sitting perfectly flat in the foam in the project boxes.

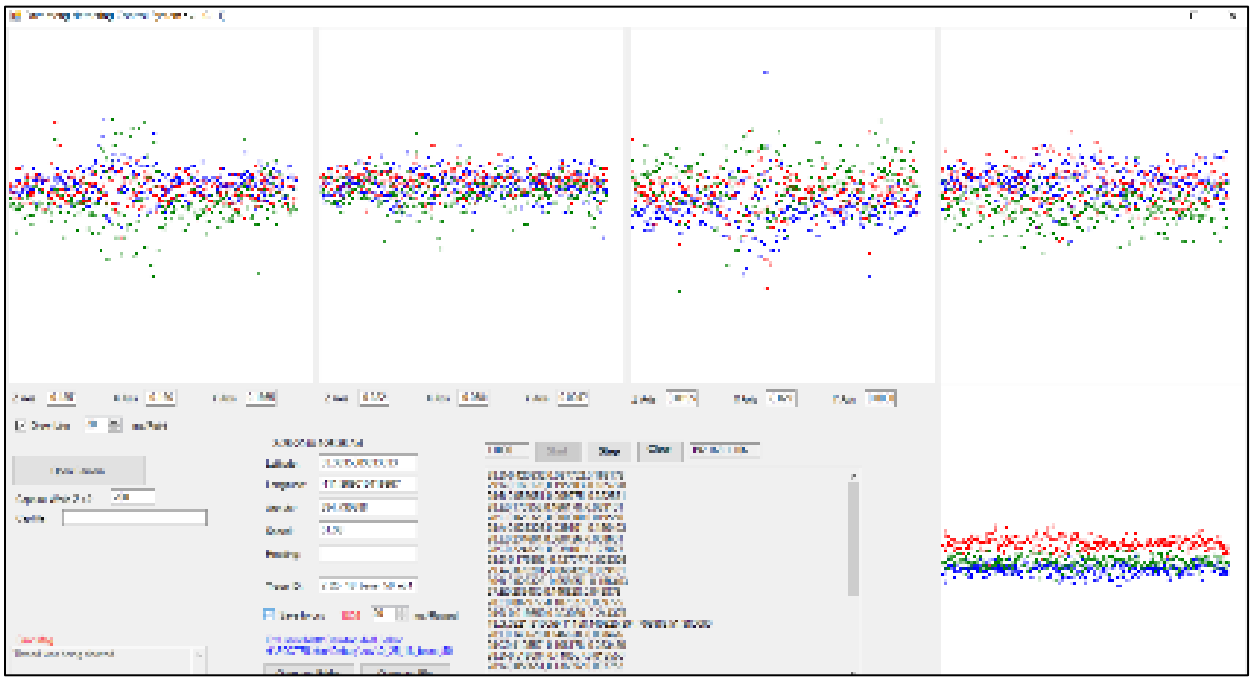

***Figure 9**: GUI during road test traveling at 60-mph.*

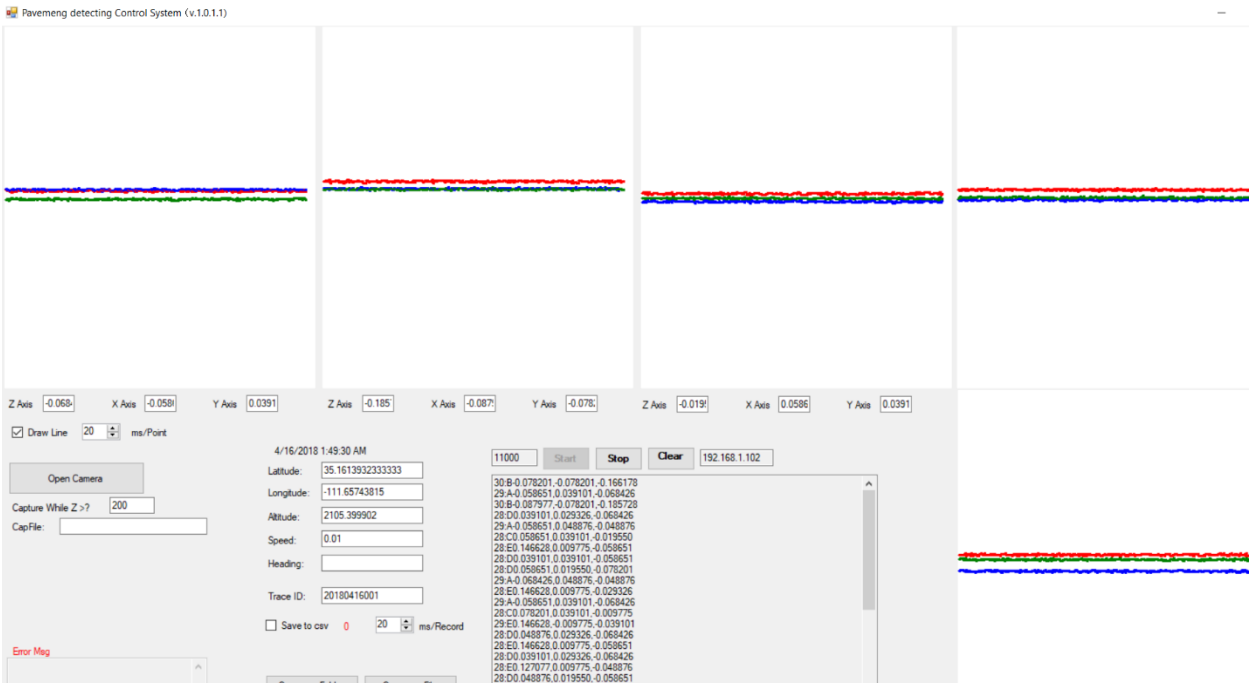

***Figure 10**: GUI during road test traveling at 0-mph.*

A GoPro Hero5 is used to confirm pavement distresses and filter out false calls such as construction joints. The GoPro Hero5 also has a built in GPS, speed tracker, and gyroscope that can be used to confirm the data that was collected with the vehicle-based sensors. When mapping severe and moderate cracking locations, a picture of the actual crack is provided from the GoPro. That way, highway agencies receive visual confirmation of the individual pavement distresses that were detected with the accelerometers. The picture shown in Figure 10 was shot at the data collection speed of 60-mph. The GoPro was mounted on the rear bumper as to capture the pavement distress right after it has been hit. When testing at night, there is not enough light to capture the frames per second. Therefore, GoPro footage is captured during the day and then the GPS metadata from the GoPro can be extracted and compared to the Adafruit Ultimate GPS component. The cost of a GoPro Hero5 is currently $200.00.

***Figure 11**: GoPro Hero5 display.*

3.2 Study Location

Two study corridors, Figure 11, were chosen in Phoenix, Arizona. Interstate 10 in Phoenix, AZ was ultimately chosen because this project was funded by ABOR as part of a tri-university project where the entire team focused their transportation research to the freight corridor of Interstate 10. However, this site was also chosen because of the hot temperatures the region receives. The terrain experiences the urban heat island effect and is covered by asphalt concrete with flat grades and an elevation of 1086-ft. The two sites on Interstate 10 were chosen based on traffic volume, differing pavement roughness, and relatively straight travel paths. The first corridor, 27th Avenue through 51st Avenue, and the second, Baseline Road through Chandler Boulevard. In 2016, the average annual daily traffic (AADT) including both east and west bound directions were approximately 186,000 vehicles per day for the Baseline Ave. – Chandler Blvd. section and 230,000 vehicles per day for the 27th Ave. – 51st Ave. section.

The 1st and 2nd right lanes were surveyed going east and west bound directions for a total of four tests per study corridor. The target testing speed was 60-mph as to remain within a safe speed while testing. Also, it has been recommended in the past that testing speeds should be selected such that the roughness measurement reflects that seen by normal traffic [7]. Because traffic congestion was an issue in these areas, tests were mostly conducted around midnight. 12 months of data was collected from February 2017 through February 2018 recording pavement conditions from a temperature range of 40ºF - 150ºF. The goal is to find a correlation between pavement roughness and pavement temperature that can be detected with vibration sensors.

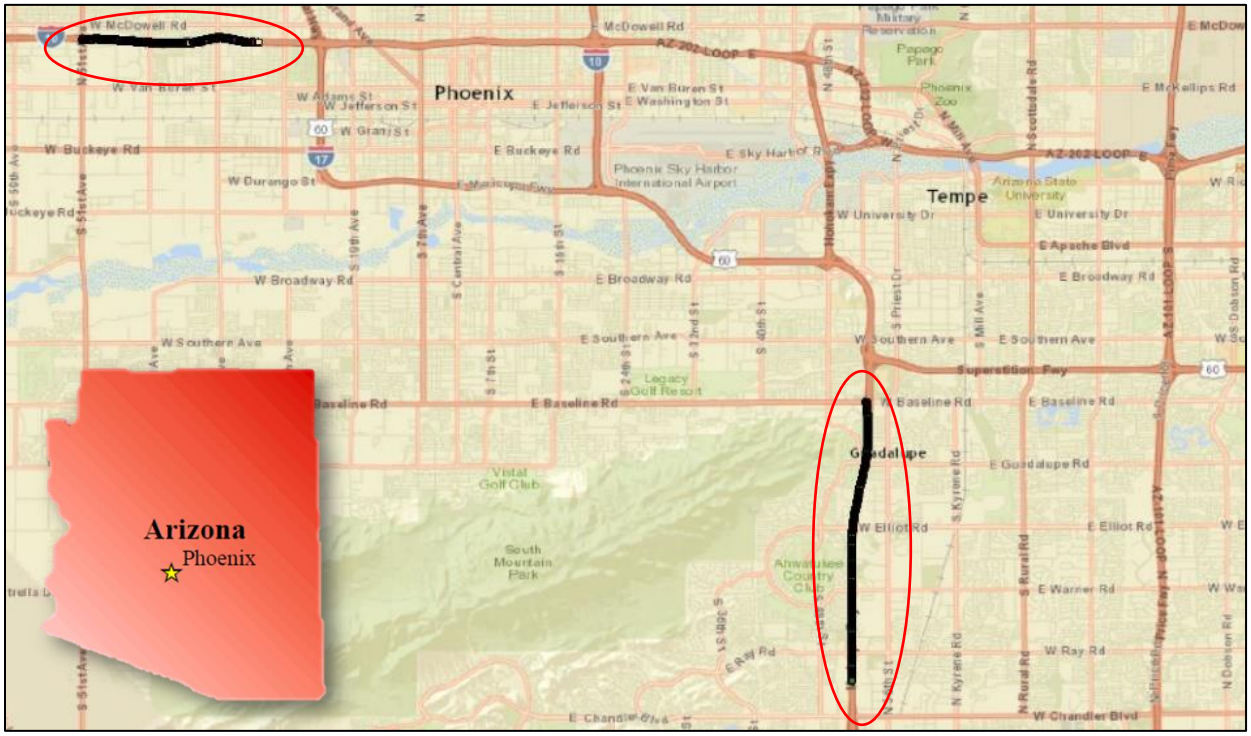

***Figure 11**: Road test site. Phoenix, AZ. 27th Ave. - 51st Ave. and Baseline Rd. - Chandler Blvd.*

4.0 Results

The data output is in acceleration of gravity in the x, y, and z-directions. The z-direction corresponds to the vertical motion of the wheel caused by a bump or change in slope of the road, the x-direction corresponds to the vehicle accelerating and braking, and the y-direction corresponds to the vehicle turning left or right. However, when a car passes over rough pavement the sensor on the wheel's control arm can shake in all directions, not just in the z-direction. While most studies only examined the forces in the z-direction, this experiment examined the total magnitude, M. of all forces for each sensor on all tests.

$$M = \sqrt{x^2 + y^2 + z^2}\,,$$

The x and y forces could be included because the vehicle speed was set to cruise control at 60-mph and the test sections were relatively straight, so the vehicle was not making drastic left or

right turns. This is also helpful in determining the size of an individual crack as when looking at the results from the z – direction there is both a positive and negative feedback from a bump.

The results showed that pavement distresses could be successfully observed by the sensors. There are spikes in the graphs where major cracks appear and the overall noise in-between the spikes give an idea of general roughness. Depending on how big the spikes are in the graph are, pavement deficiencies could be classified, linked with GPS, and later georeferenced onto a map. The effects of temperature were noticed by sensors on the wheels, but not so much by the sensors inside the vehicle. This could be because of tire pressure changes and the suspension system of the vehicle.

4.1 Threshold method

This project aimed to create a system that identifies individual cracks that could hold significant weight in determination of IRI. To do this, it was necessary to classify individual pavement distresses as moderate or severe based on examination of the data outputs. After examining the raw data, threshold values for severe and moderate cracking were chosen and monitored over the length of the experiment. Values above this threshold were filtered and graphed against temperature as well as mapped in ArcGIS.

An example of choosing threshold based on the raw data is shown in Figure 12. Moderate cracks were said to have a threshold of 1.5 times the force of gravity while severe cracks were above 2.5 times the force of gravity. These values were chosen based on engineering judgement.

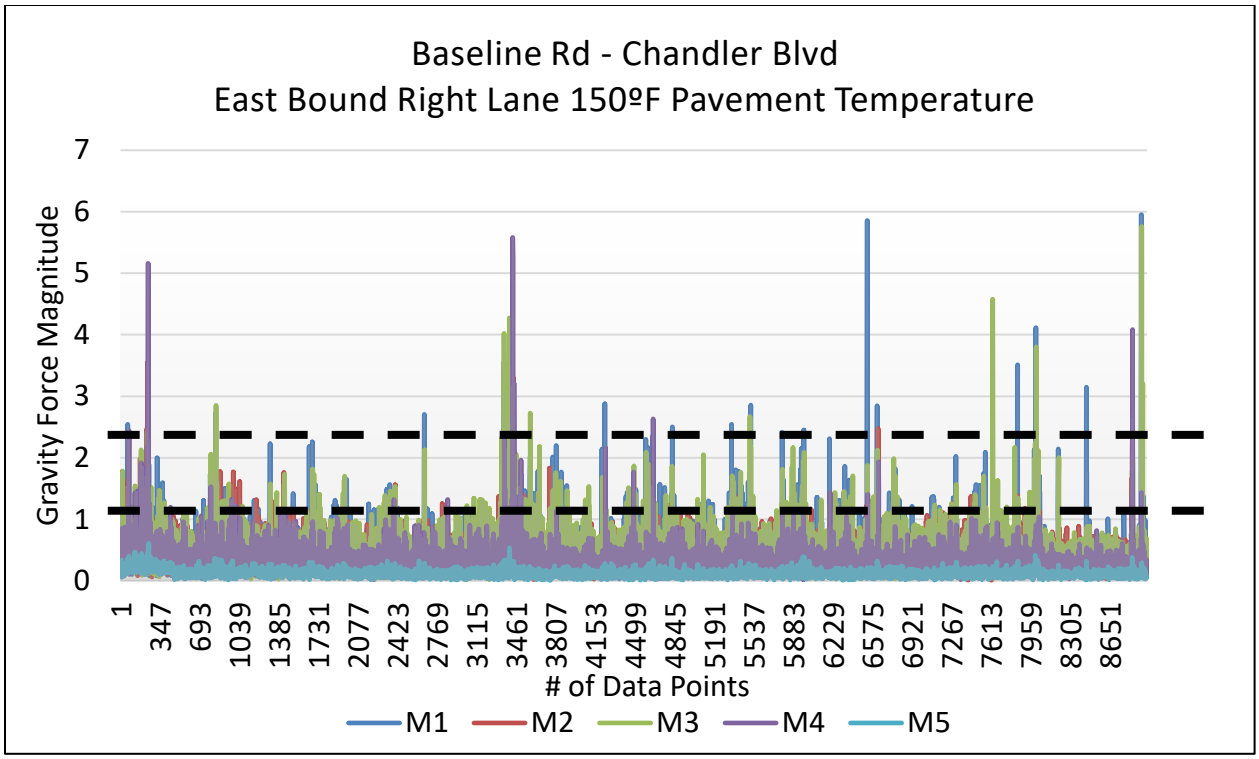

***Figure 12**: Using the Threshold method on raw data.*

M1, M2, M3, M4, and M5 correspond to the magnitude of each sensor, M5 being the sensor inside the vehicle. The threshold can be switched depending on which sensor is being observed. For example, the M5 sensor would require lower threshold values to identify severe cracks. Also, sensors M1-M4 can be averaged, i.e. M(1-4)avg. and the threshold can be adjusted according to engineering judgement.

The following Figures 13 & 14 were produced using a threshold value of 1.0g to show a relationship between temperature and vibration. This threshold was chosen to observe the overall noise of the road and not just the severe and moderate cracks. The temperature vs. gravity graphs are a compilation of all eight road tests and all five accelerometers. A trend is shown that as temperature increases, vibration increases. The iPhone sensor, as well as the accelerometer inside the vehicle, did not show this trend.

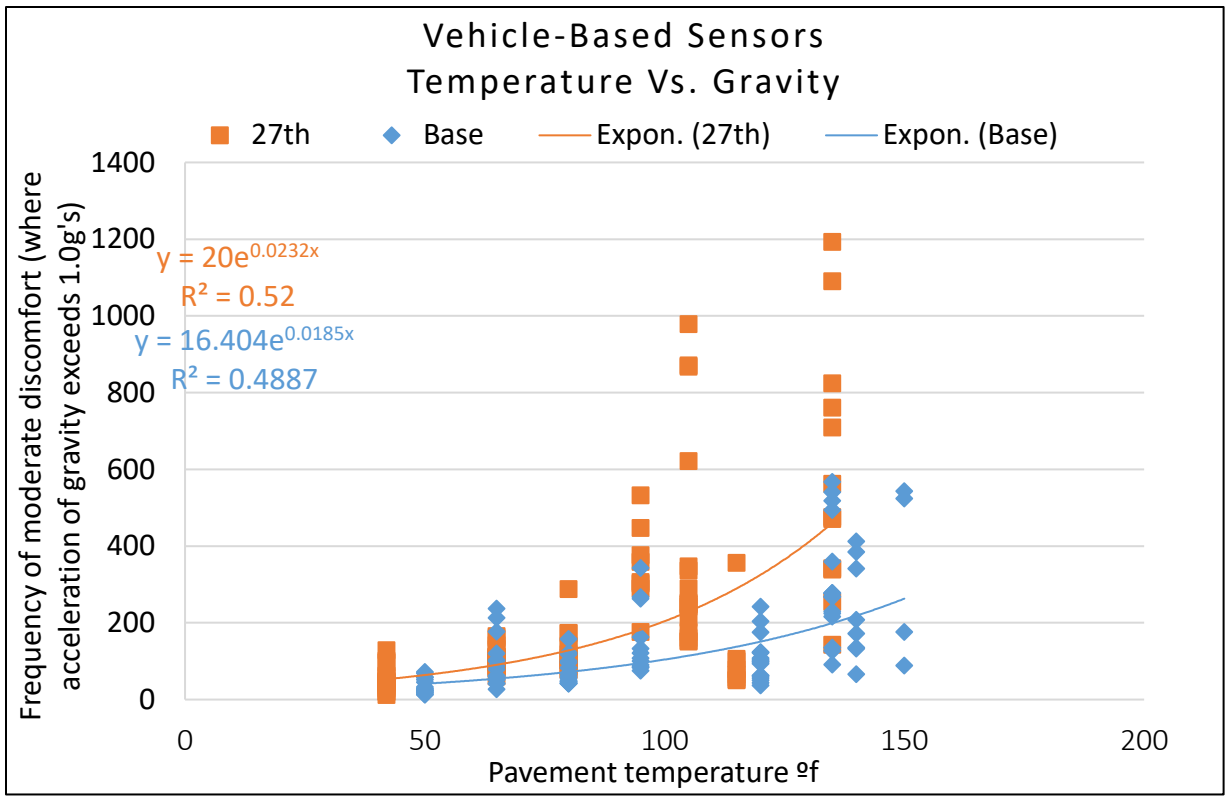

***Figure 14**: Threshold method showing how vibration increases with temperature.*

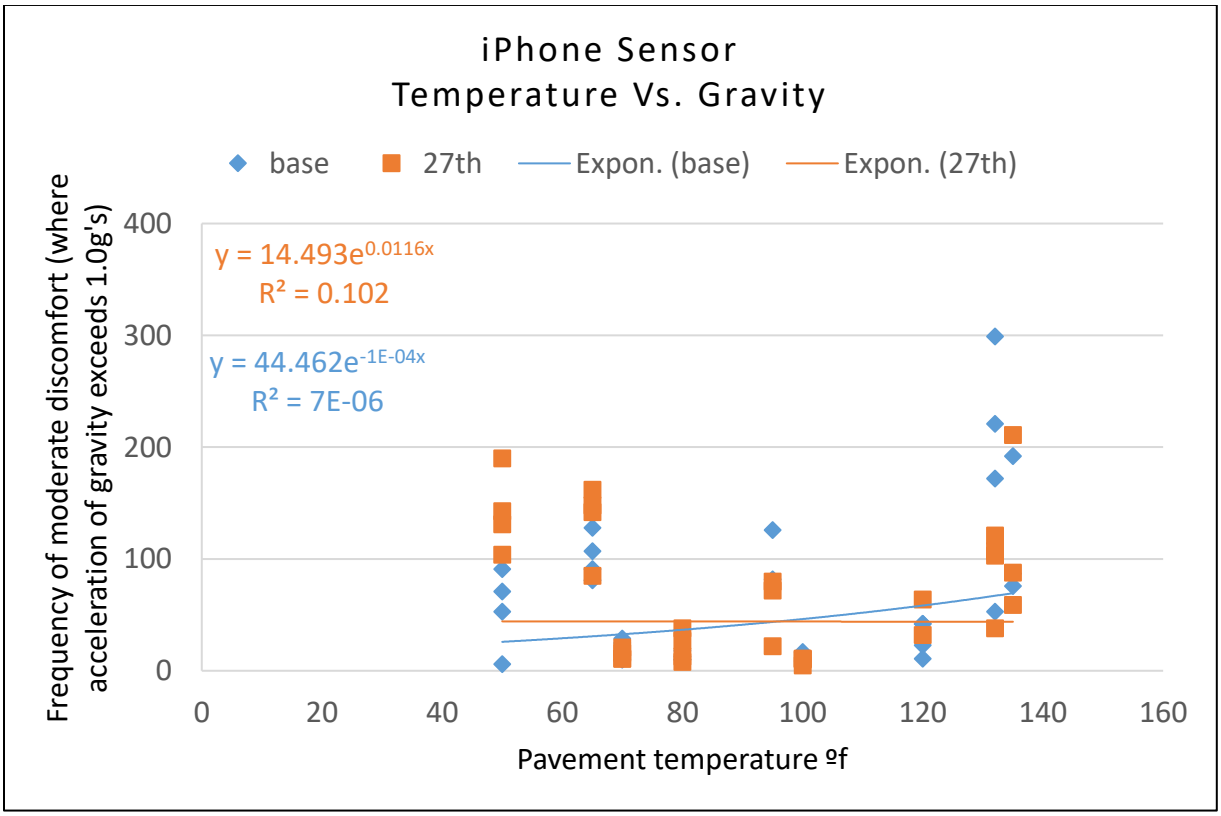

***Figure 14**: Threshold method – smartphone sensor does not sense change in temperature.*

These results are startling at first because one would expect smoother conditions at hot temperatures. When an asphalt pavement is subject to hot temperatures, it acts more like a liquid then at cool temperatures. Since the pavement is more likely to deform at hotter temperatures it makes intuitive sense that there would be more vibration. The tires air pressure is also a suspect for this trend. Tire pressure changes with temperature and could be the reason that this trend is observed. This phenomenon of tire pressure is explored later in this document. Figures 13 & 14 only look at data collected for half of a year as to exclude increased vibration due to pavement deterioration.

To observe how vibration changes due to temperature variation and deterioration over a full year, Figures 15 - 22 were created with a secondary axis of pavement temperature. The following figures are the eight test sections with the magnitude of each sensor graphed against pavement temperature and corresponding month. The blue area chart represents the pavement temperatures during the tests while the line charts represent each sensor. The pavement temperature is on the right vertical axis while the vibration is expressed on the left vertical axis. There are some gaps in the data due to technical difficuilties during testing such as poor connections with WiFi. After observing all the graphs using this threshold method, a trend was noticed but it didn't always fit perfectly. It appeared that there were spikes in the line charts corresponding to higher temperatures but the team was unable to be sure without performing statistical analysis.

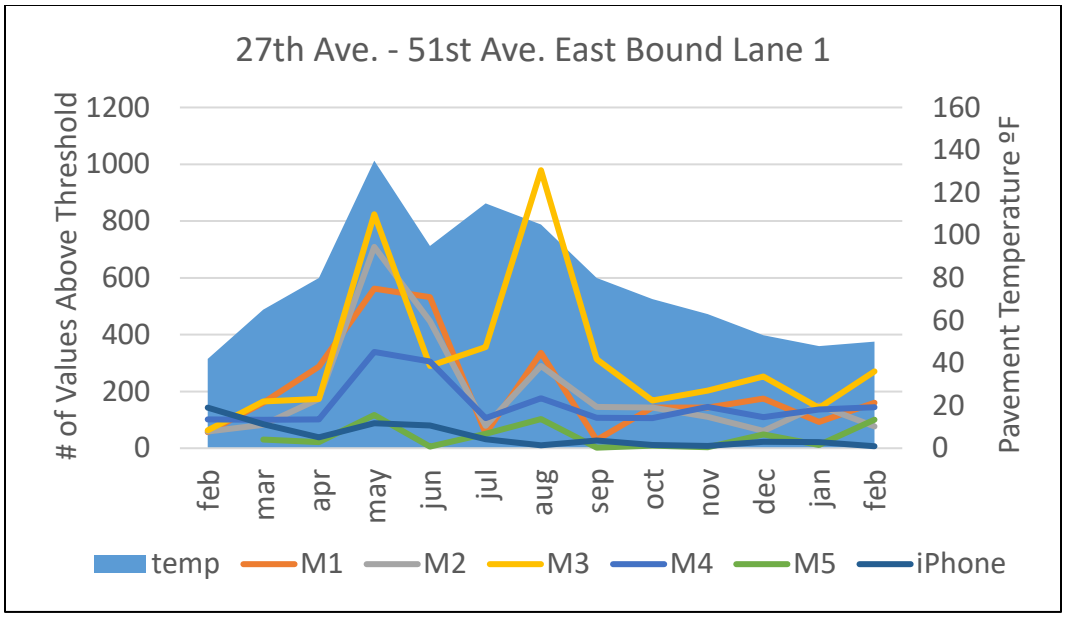

***Figure 155**: Threshold method over a year. 27th Ave. - 51st Ave. East Bound Lane 1.*

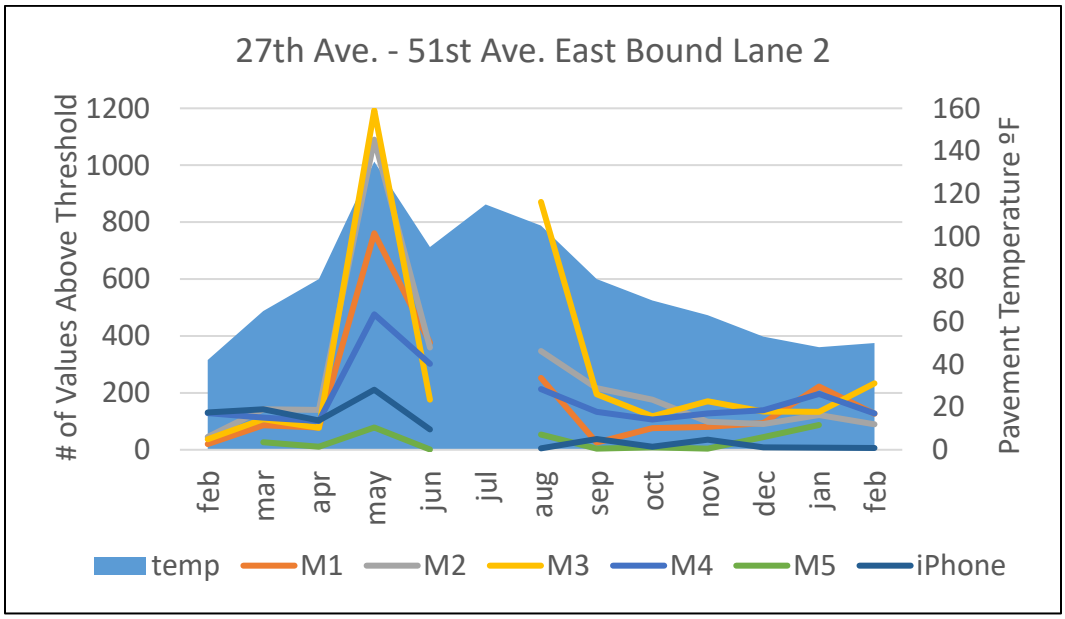

***Figure 16**: Threshold method over a year. 27th Ave. - 51st Ave. East Bound Lane 2.*

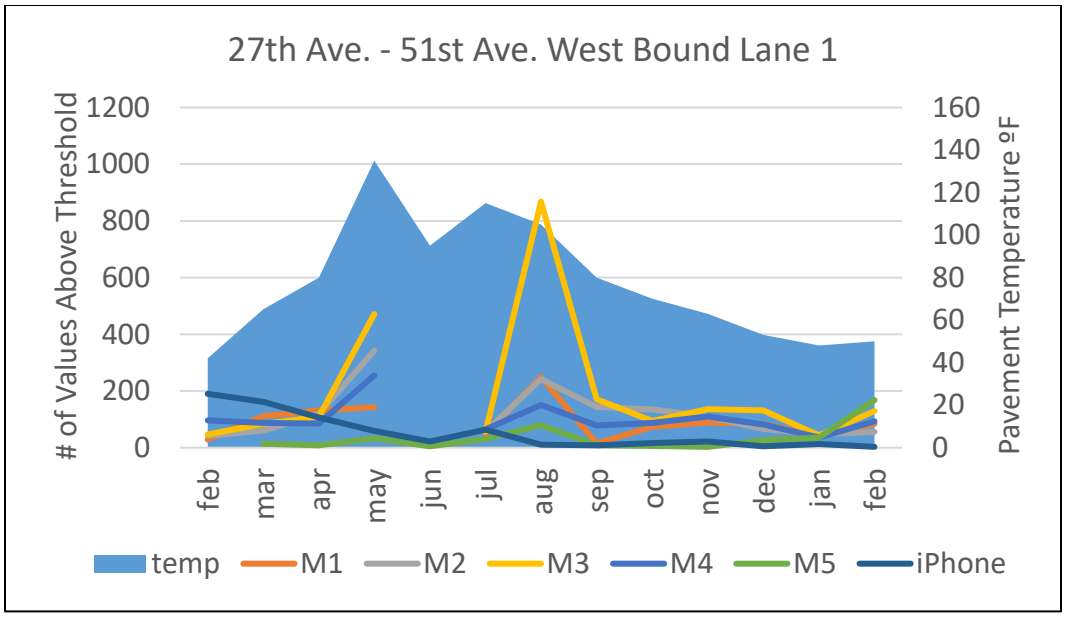

***Figure 167**: Threshold method over a year. 27th Ave. - 51st Ave. West Bound Lane 1.*

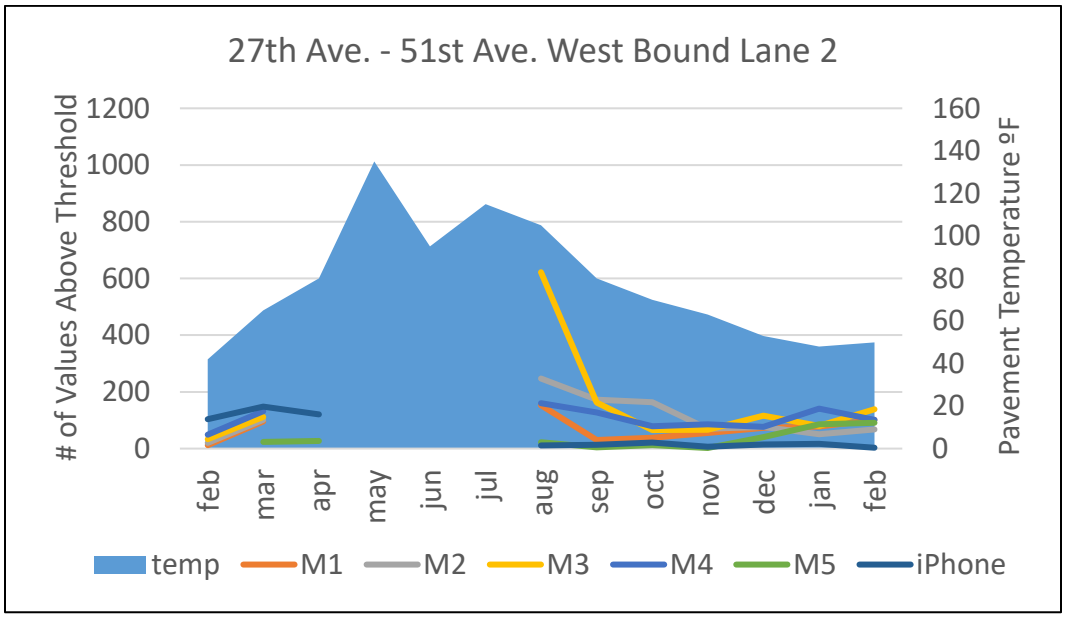

***Figure 18**: Threshold method over a year. 27th Ave. - 51st Ave. West Bound Lane 2.*

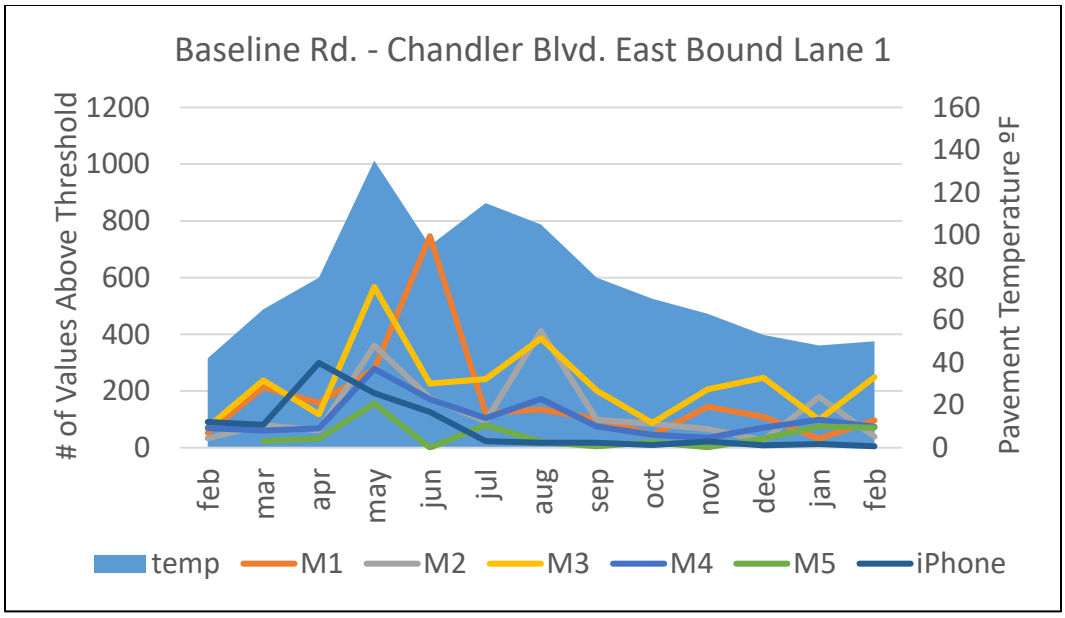

***Figure 179**: Threshold method over a year. Baseline Rd. - Chandler Blvd. East Bound Lane 1.*

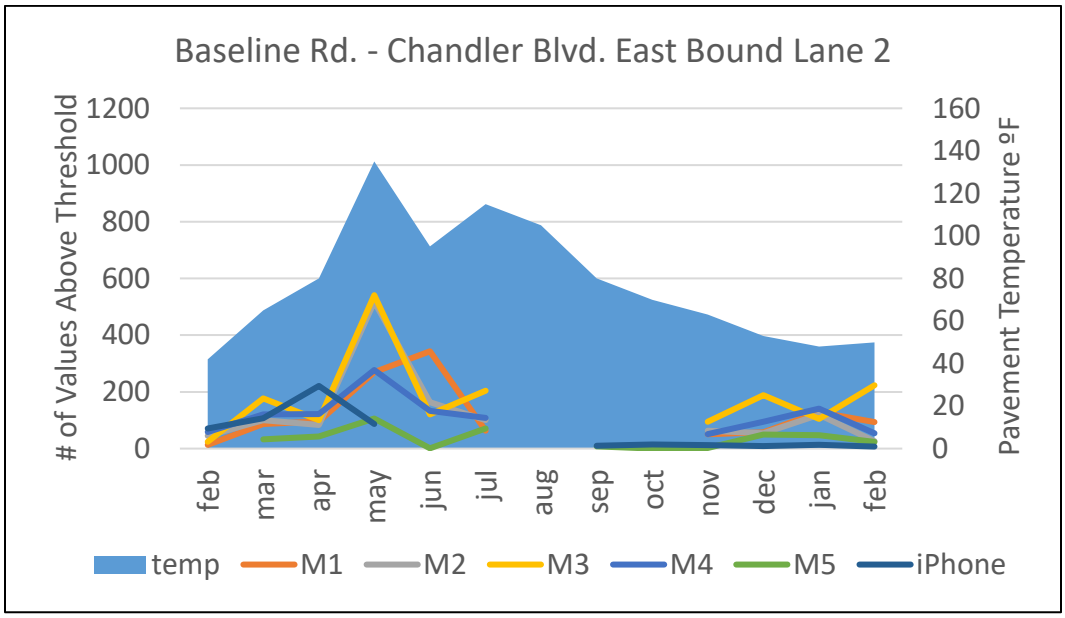

***Figure 180**: Threshold method over a year Baseline Rd. - Chandler Blvd. East Bound Lane 2.*

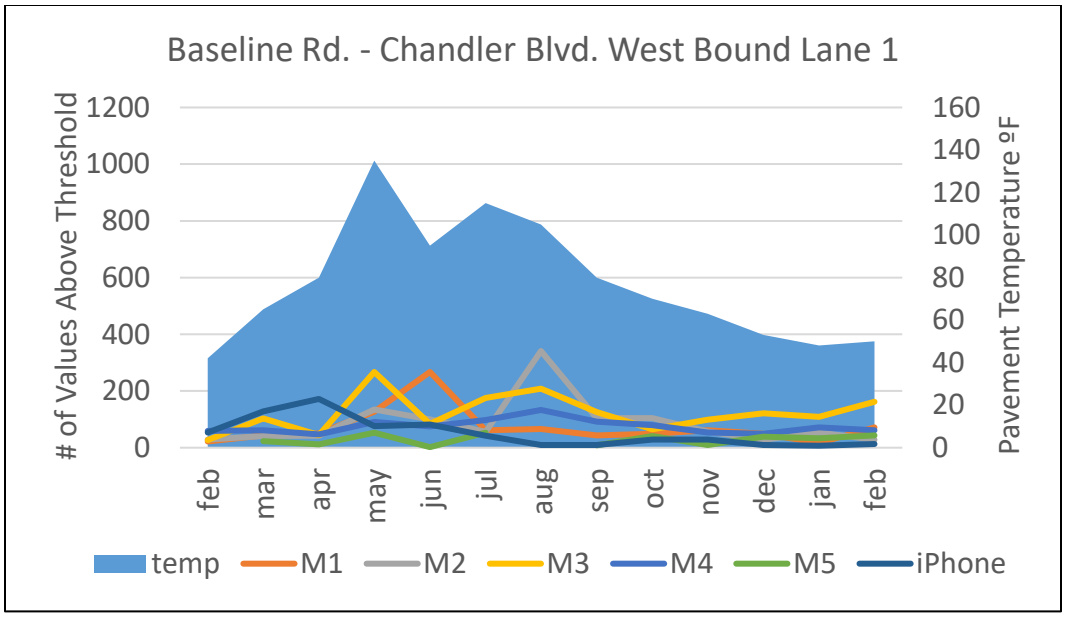

***Figure 21**: Threshold method over a year. Baseline Rd. - Chandler Blvd. West Bound Lane 1.*

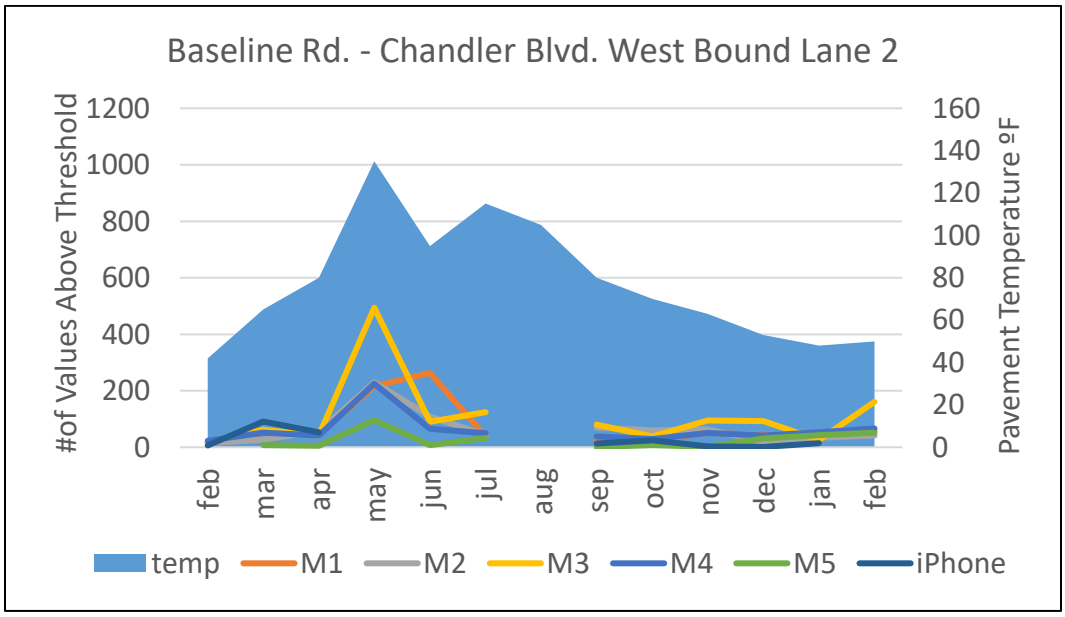

***Figure 192**: Threshold method over a year. Baseline Rd. - Chandler Blvd. West Bound Lane 2.*

4.2 Average Method

Another method was used to observe if temperature has significant effect on vibration. The average method was performed by taking the overall average of each sensors and graphing them against temperature. Each sensor's magnitude was averaged over the complete time duration of each of the eight testing sections. The following Figures 23-30 show the average method for each of the eight test sections. The average of each sensor was graphed against pavement temperature and corresponding month. The graphs can be read the same way as the threshold method, with the pavement temperature as the area chart and the individual sensors as the line charts. The average method again showed a suspicious interaction between temperature and vibration, but the relationship was not as prevalent as the threshold above. The iPhone sensors average especially did not show any signs of relationship with temperature and vibration but the sensor inside the vehicle appeared to go back and forth in no significant pattern.

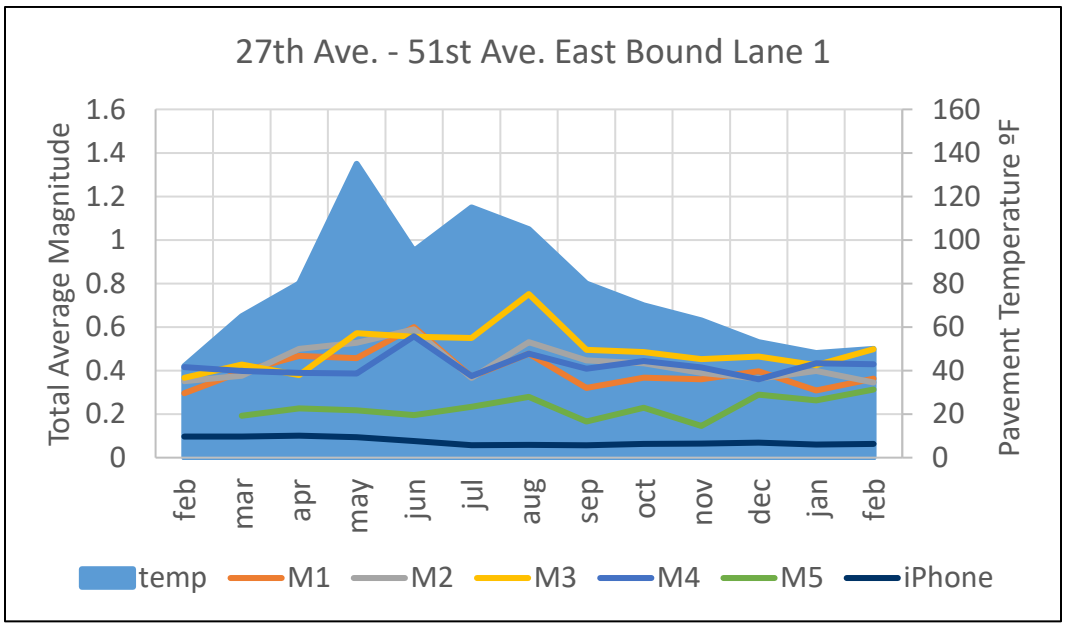

***Figure 23**: Average method over a year. 27th Ave. - 51st Ave. East Bound Lane 1.*

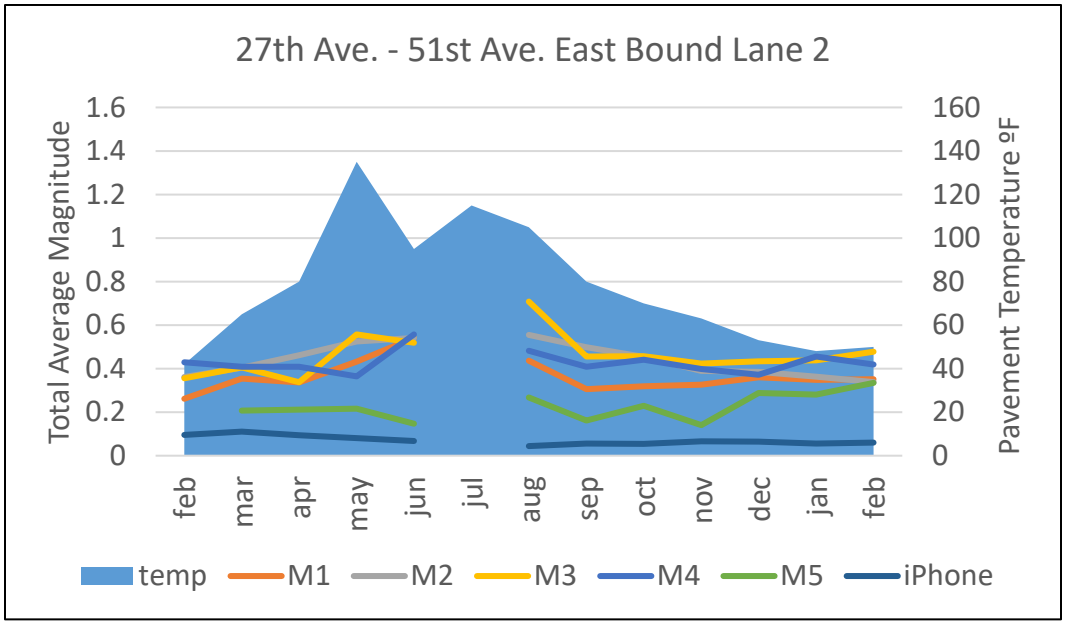

***Figure 204**: Average method over a year. 27th Ave. - 51st Ave. East Bound Lane 2.*

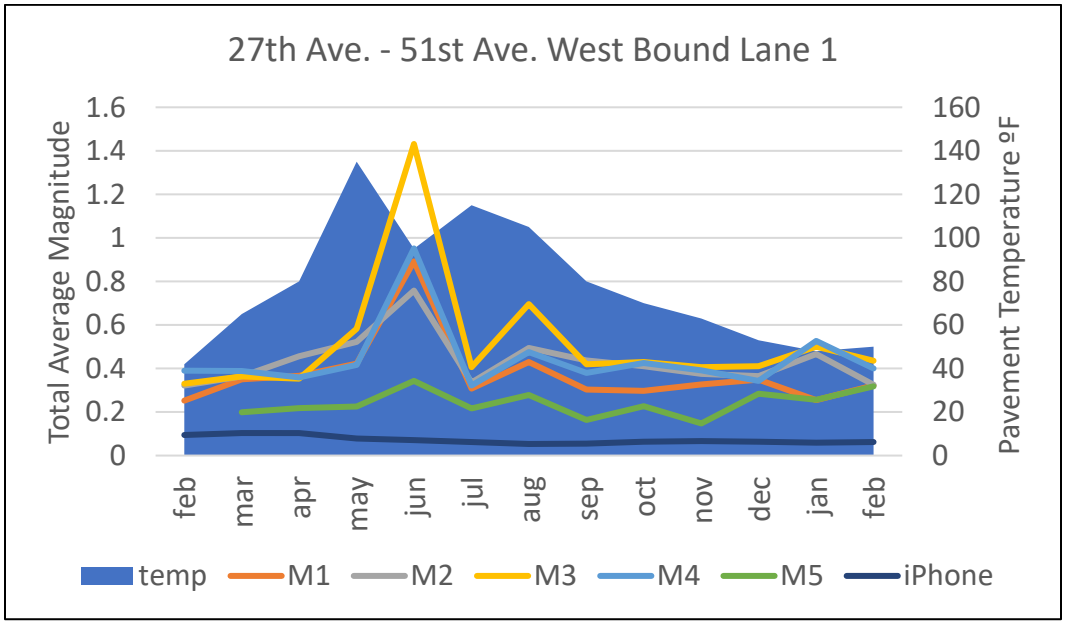

***Figure 215**: Average method over a year. 27th Ave. - 51st Ave. West Bound Lane 1.*

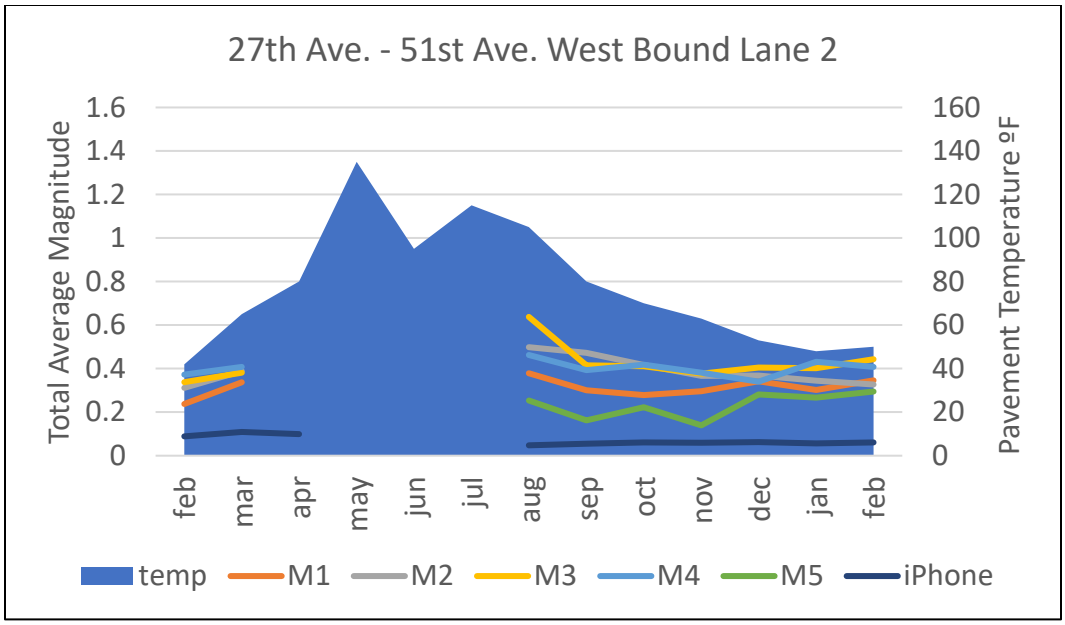

***Figure 226**: Average method over a year. 27th Ave. - 51st Ave. West Bound Lane 2.*

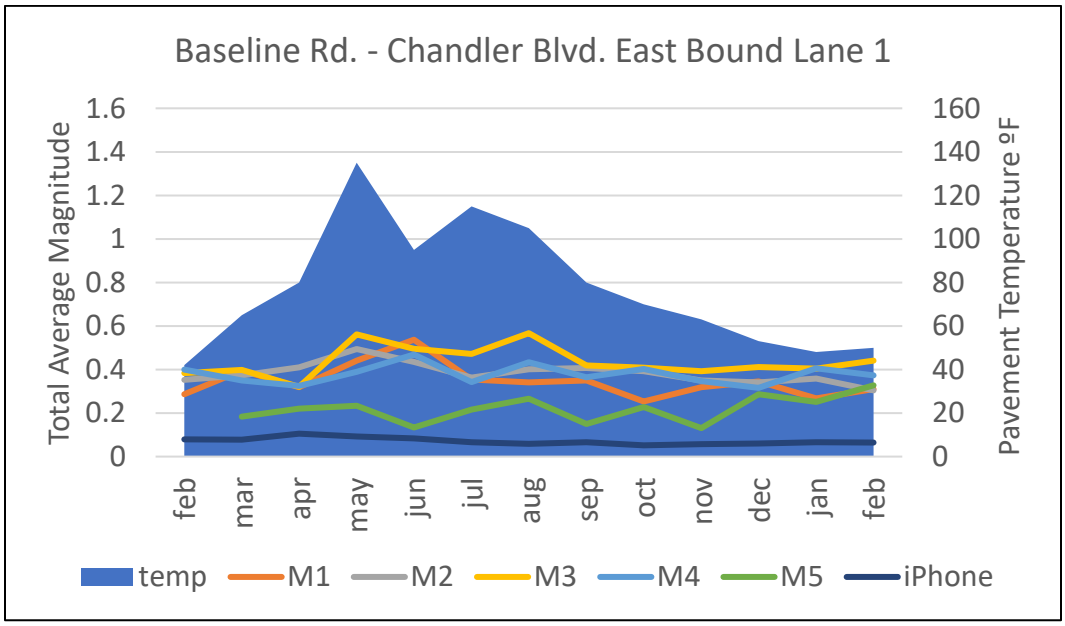

***Figure 237**: Average method over a year. Baseline Rd. - Chandler Blvd. East Bound Lane 1.*

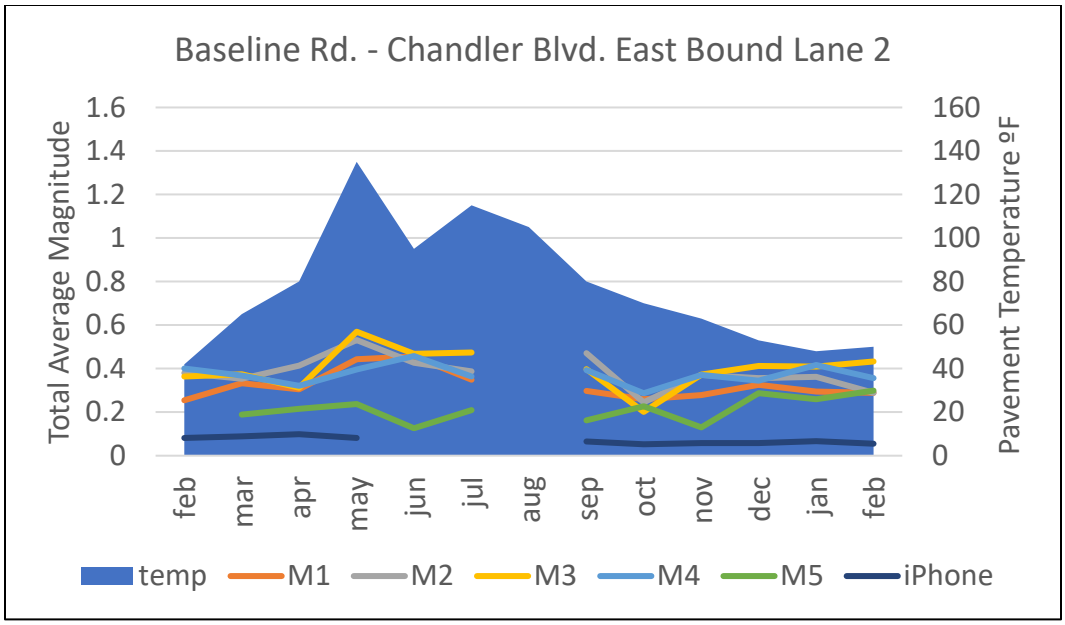

***Figure 28**: Average method over a year. Baseline Rd. - Chandler Blvd. East Bound Lane 2.*

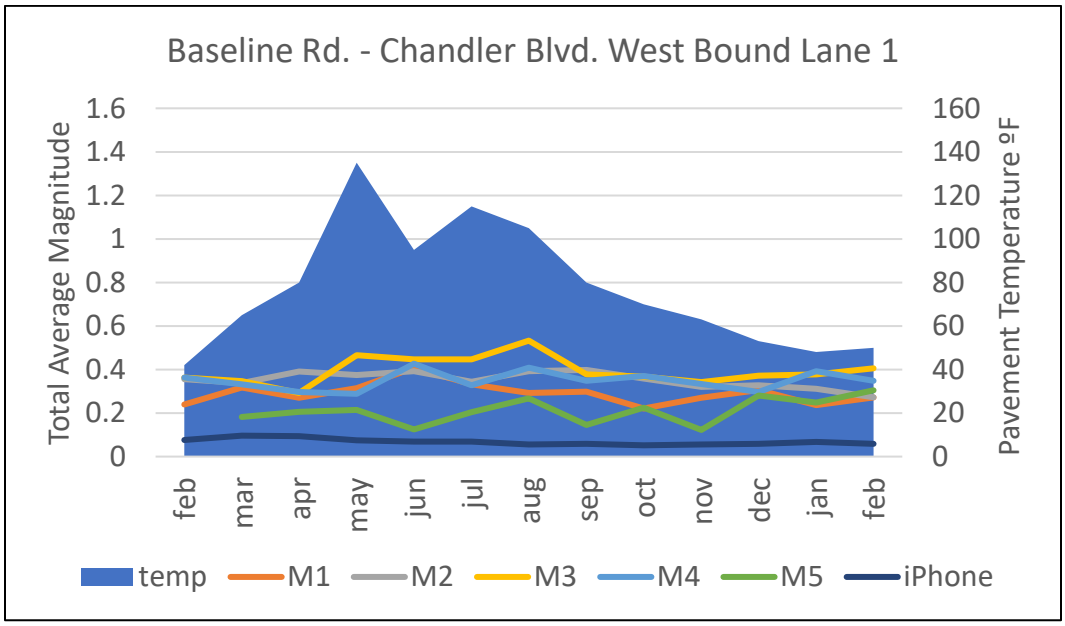

***Figure 29**: Average method over a year. Baseline Rd. - Chandler Blvd. West Bound Lane 1.*

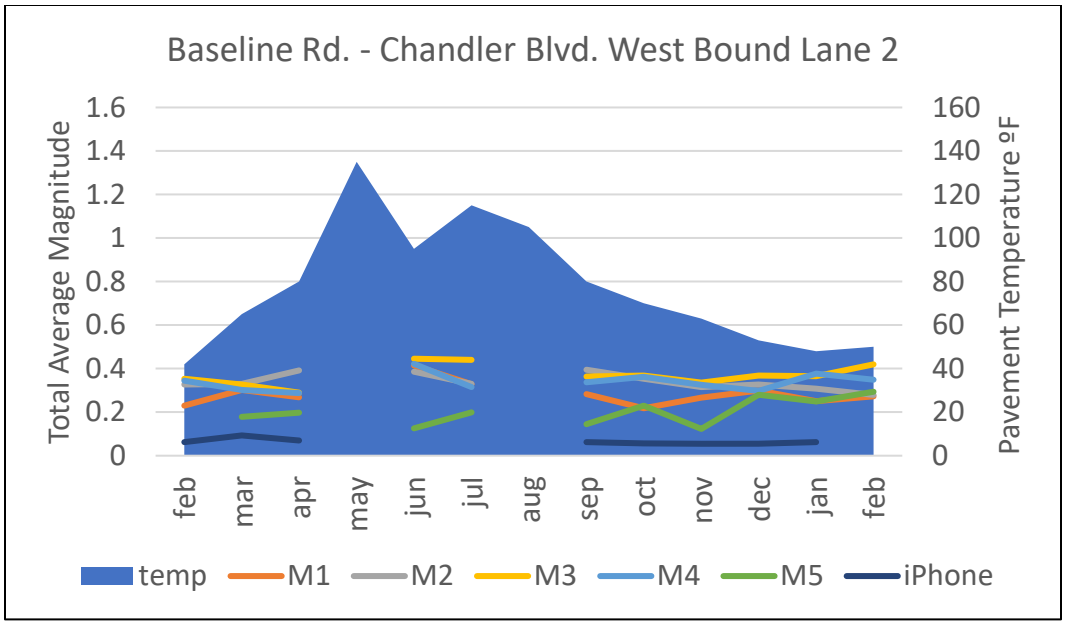

***Figure 30**: Average method over a year. Baseline Rd. - Chandler Blvd. West Bound Lane 2.*

4.3 GIS Mapping

Using ArcGIS, data was georeferenced into a useable format for highway agencies. The average of all four wheel sensors were mapped, M(1-4)avg. From inspecting the M(1-4)avg values, severe and moderate cracks were graphed based on acceleration of gravity above 0.8g and 1.0g respectively. The following maps in Figures 31-32 show the transition throughout the year by showing the months of March, June, September, and December. The results show that when temperature was hotter, there appears to be a greater increase in cracking. Some cracks that appeared as moderate in the cold, appear as severe in the heat, and the frequency of moderate cracks increases with temperature. These results were expected as the temperature-vibration trend was noticed from the raw data, but it makes it difficult to trust which is the real representation of the road and difficult to decide what is the ideal temperature for testing road roughness. 27th Ave. - 51st Ave. is shown first followed by Baseline Rd. – Chandler Blvd.

***Figure 31**: 27th Ave. – 51st Ave. Top to bottom: severe and moderate cracks for east and west bound lane 1 in March, June, September, and December.*

The hottest month of the four months, June, has the most cracking and coolest month, December, has the least even though December was one of the latest months in the year long study. The Baseline Rd. – Chandler Blvd. maps are shown below enlarged to observe the detail.

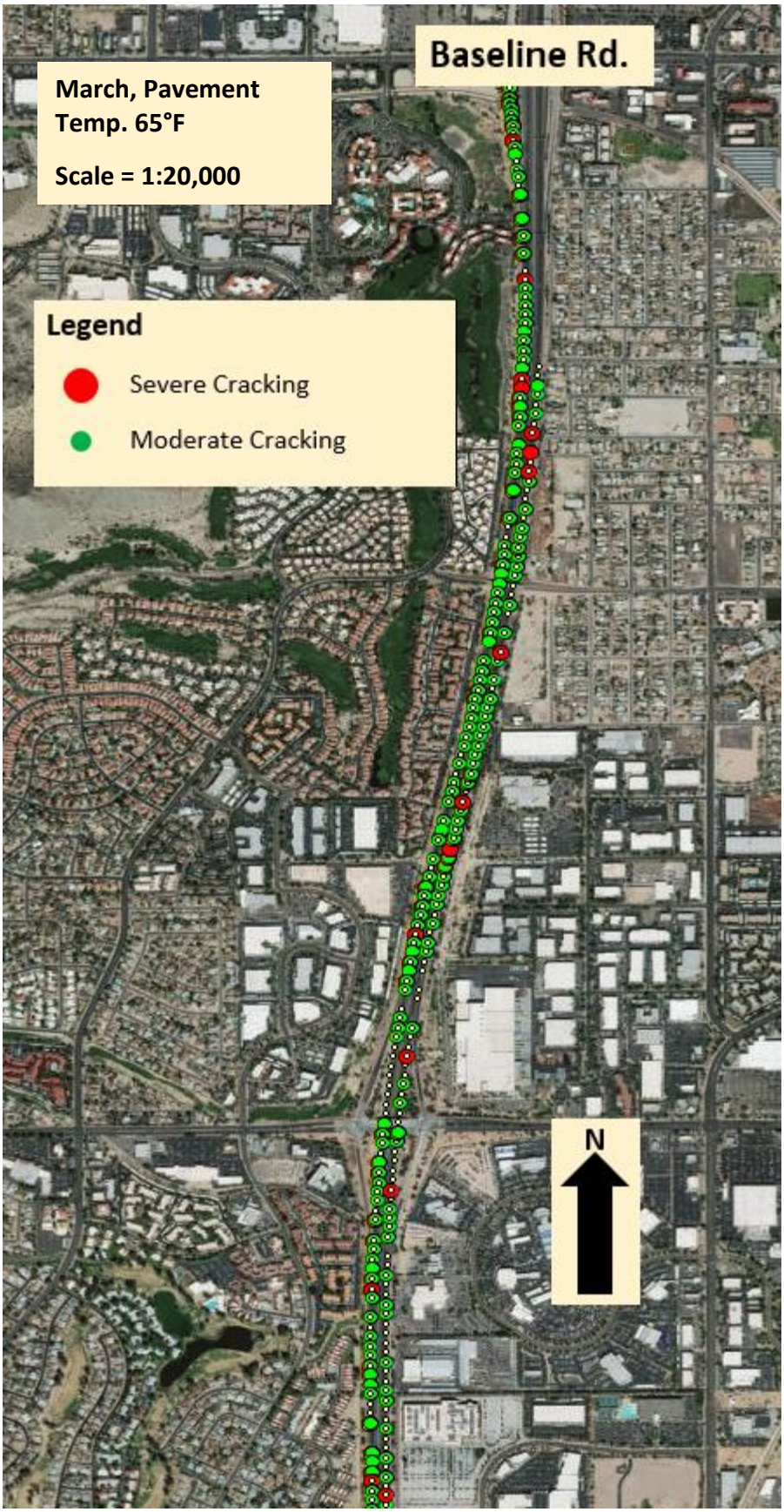
Baseline Rd.
March, Pavement Temp. 65°F
Scale = 1:20,000
Legend
Severe Cracking
Moderate Cracking
N

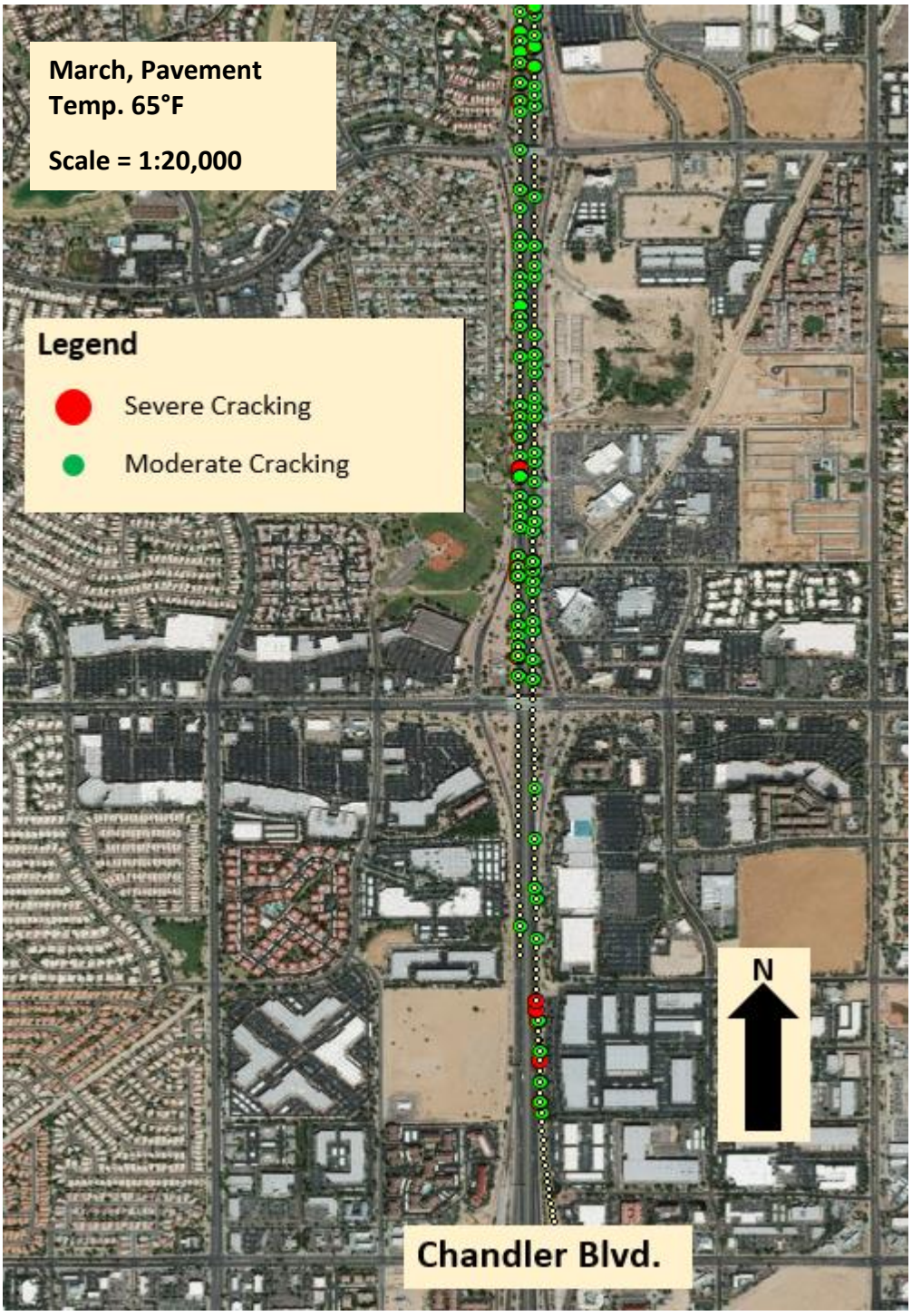
March, Pavement Temp. 65°F
Scale = 1:20,000
Legend
Severe Cracking
Moderate Cracking
N
Chandler Blvd.

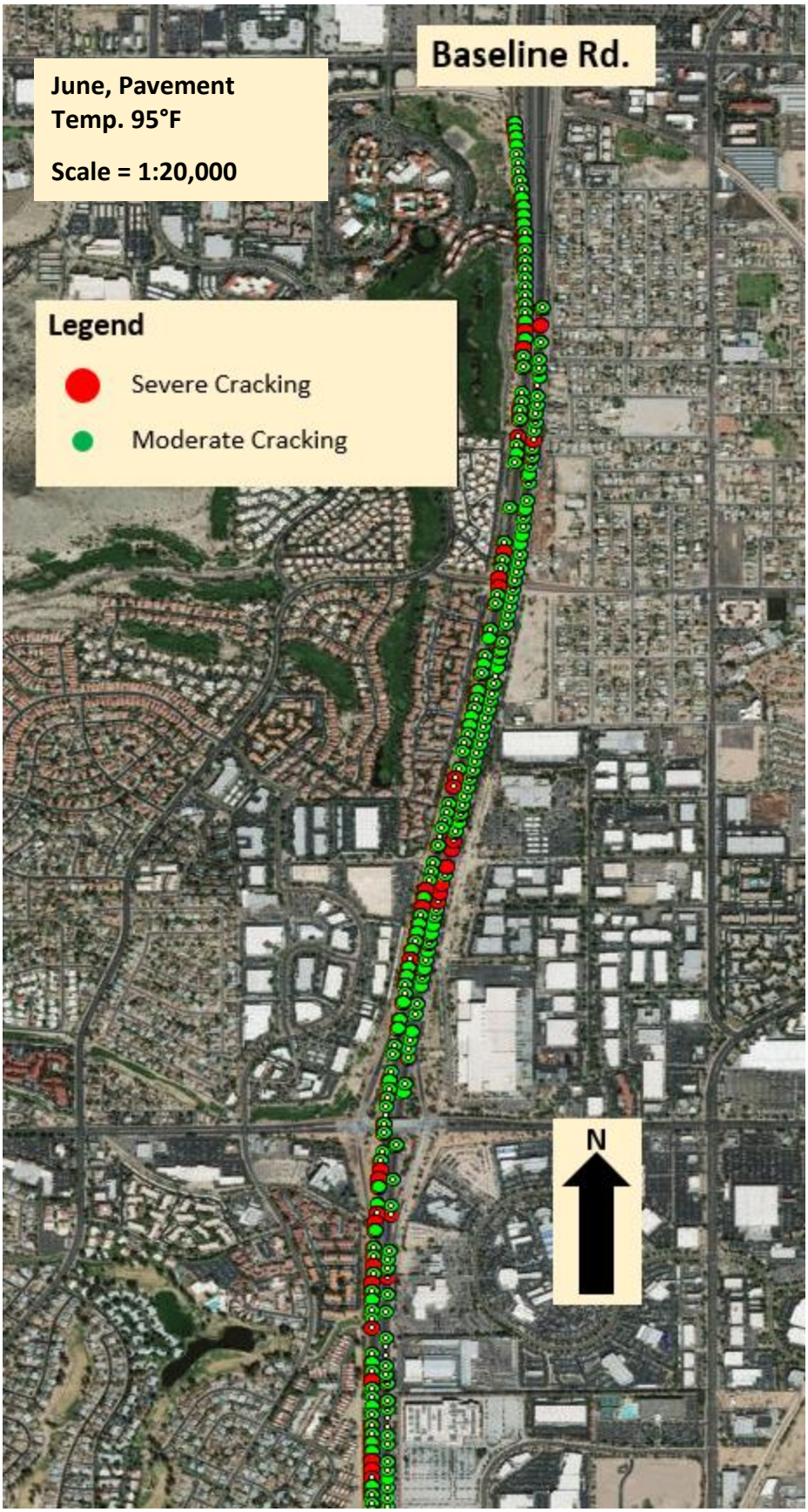
Baseline Rd.
June, Pavement Temp. 95°F
Scale = 1:20,000
Legend
Severe Cracking
Moderate Cracking
N

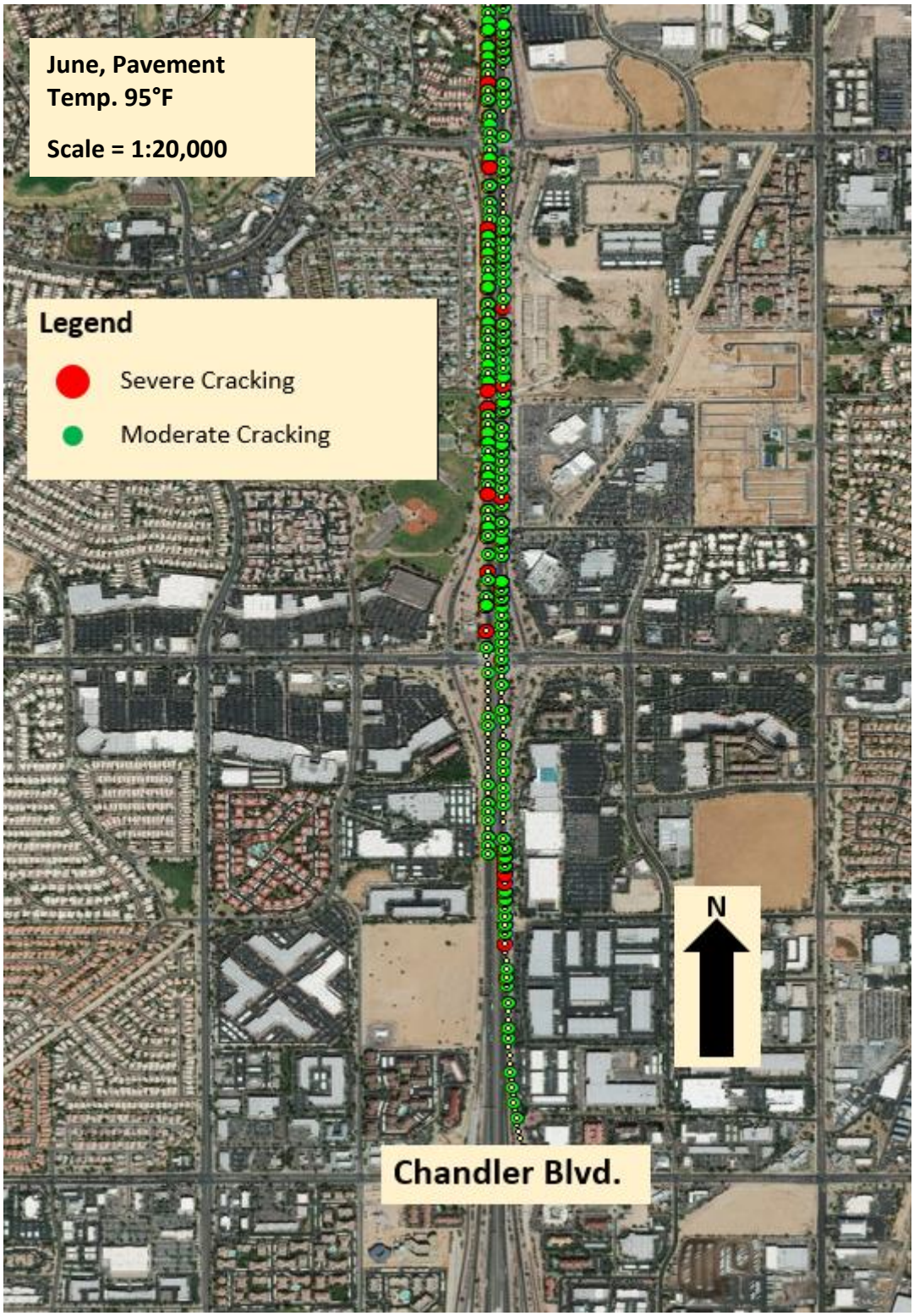
June, Pavement
Temp. 95°F
Scale = 1:20,000
Legend
Severe Cracking
Moderate Cracking
N
Chandler Blvd.

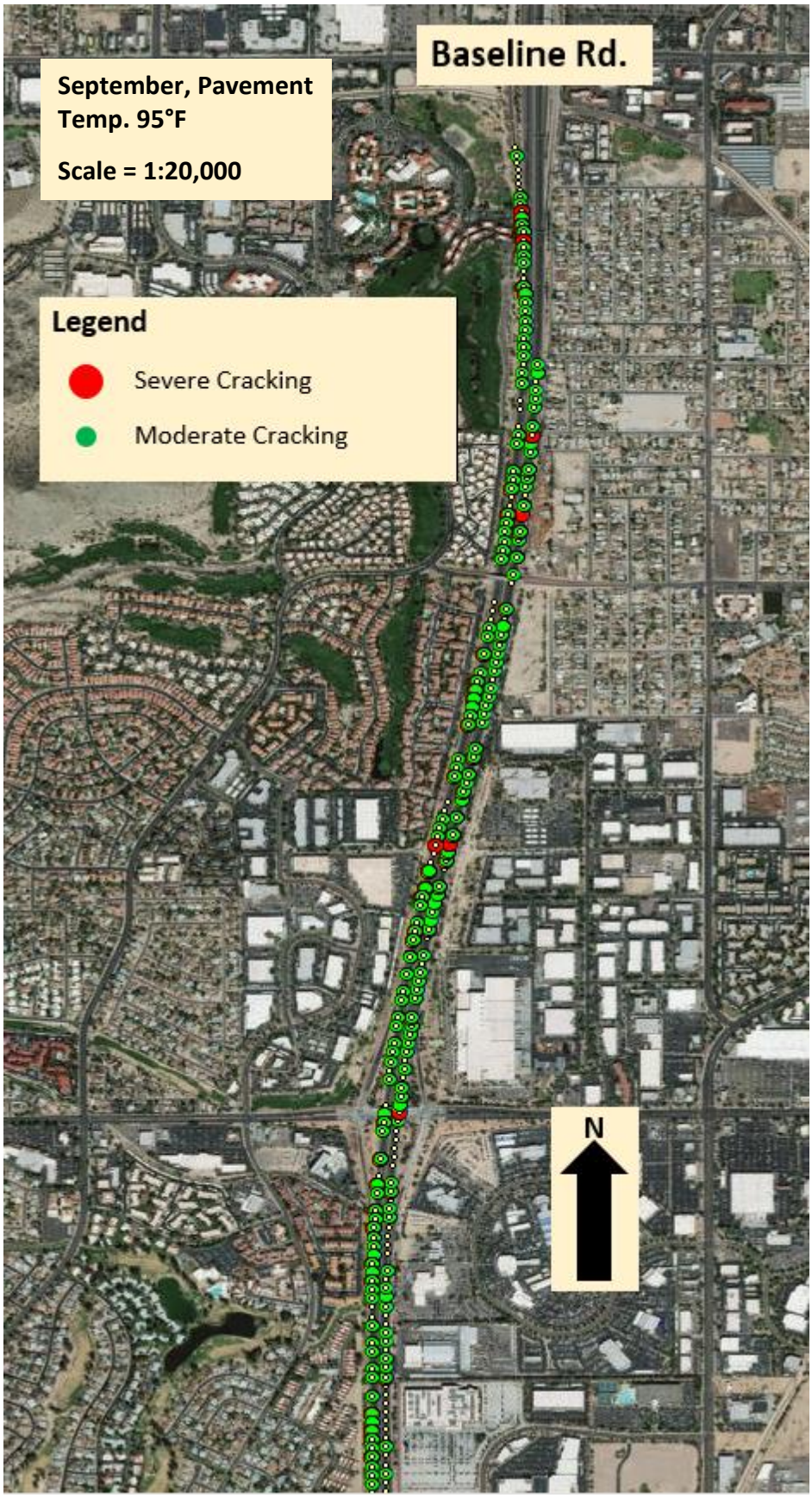
Baseline Rd.
September, Pavement Temp. 95°F
Scale = 1:20,000
Legend
Severe Cracking
Moderate Cracking
N

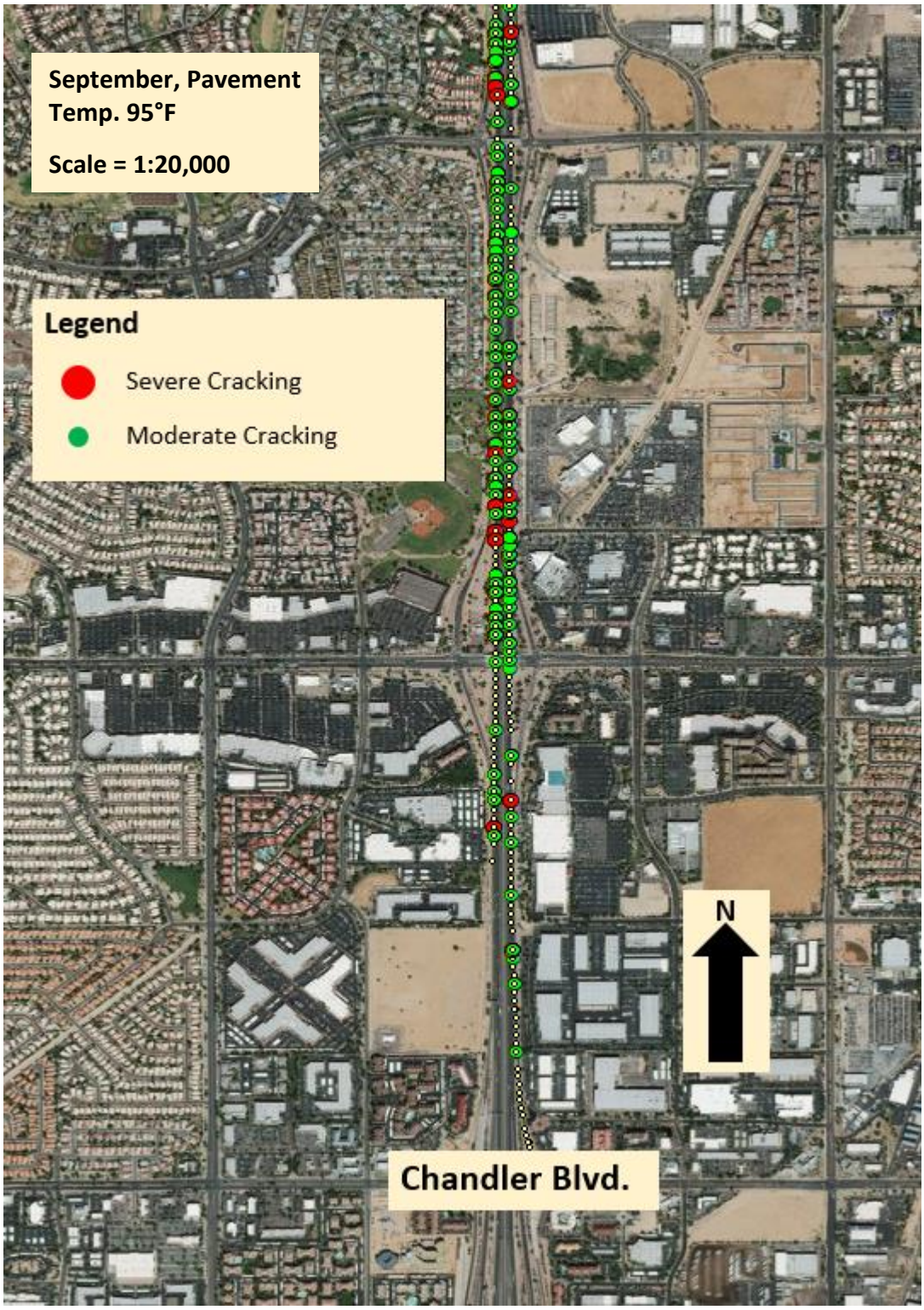
September, Pavement Temp. 95°F
Scale = 1:20,000
Legend
Severe Cracking
Moderate Cracking
N
Chandler Blvd.

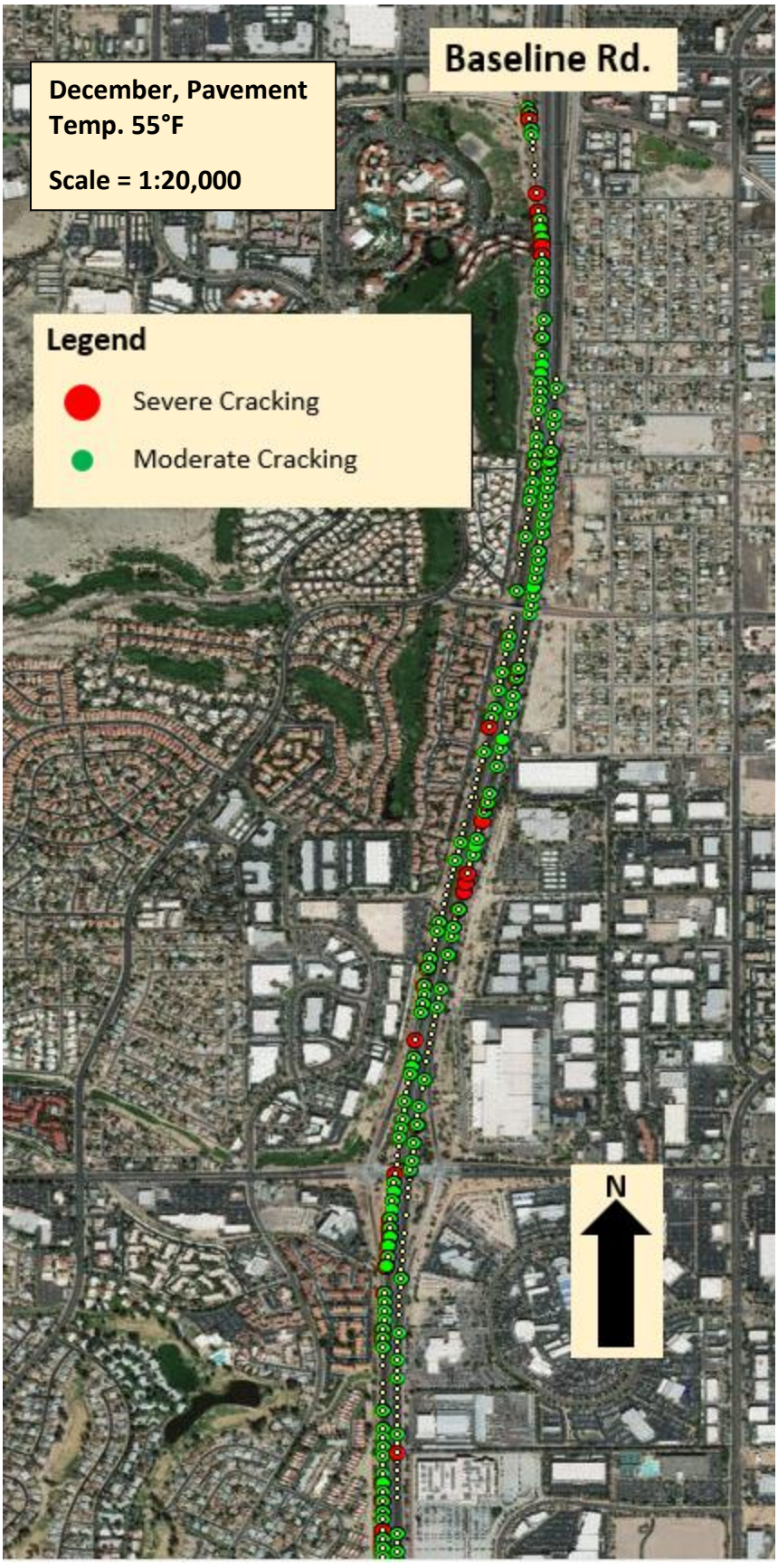
Baseline Rd.
December, Pavement Temp. 55°F
Scale = 1:20,000
Legend
Severe Cracking
Moderate Cracking
N

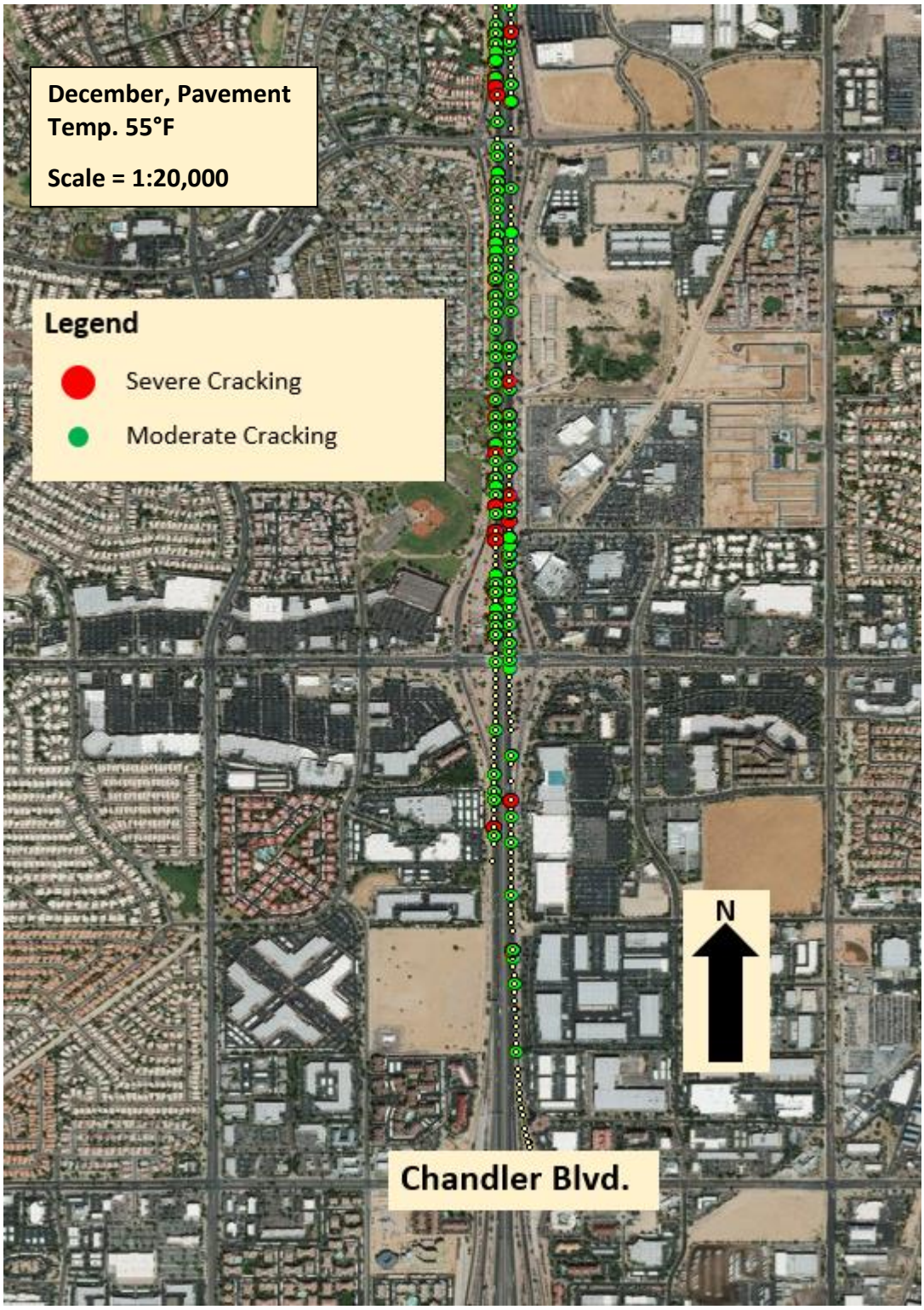

Figure 32: *Baseline Rd. – Chandler Blvd. Top to bottom: severe and moderate cracks for east and west bound lane 1 in March, June, September, and December. Figure is broken up into north and south segments for each month to view the detail.*

It is useful to compare IRI values from ADOT with the accelerometer data. Figure 33 shows ADOT IRI segment values graphed underneath the accelerometer sensors. Because IRI values are in segments, individual pavement deficiencies are not identified. By overlaying these two methods on top of each other, highway agencies can determine if certain severe cracks are holding significant weight in the reported IRI. Ideally, all this information would get mapped with picture links for each severe or moderate crack. However, depending on temperature the amount of cracking could go up or down. ADOT does not report temperatures at which IRI values were recorded. Therefore, it is recommended to use accelerometer vehicle-based sensors during the average temperature that the region receives. This data could be made public on a website for travelers to be prepared for the type of roughness their vehicles are going to encounter.

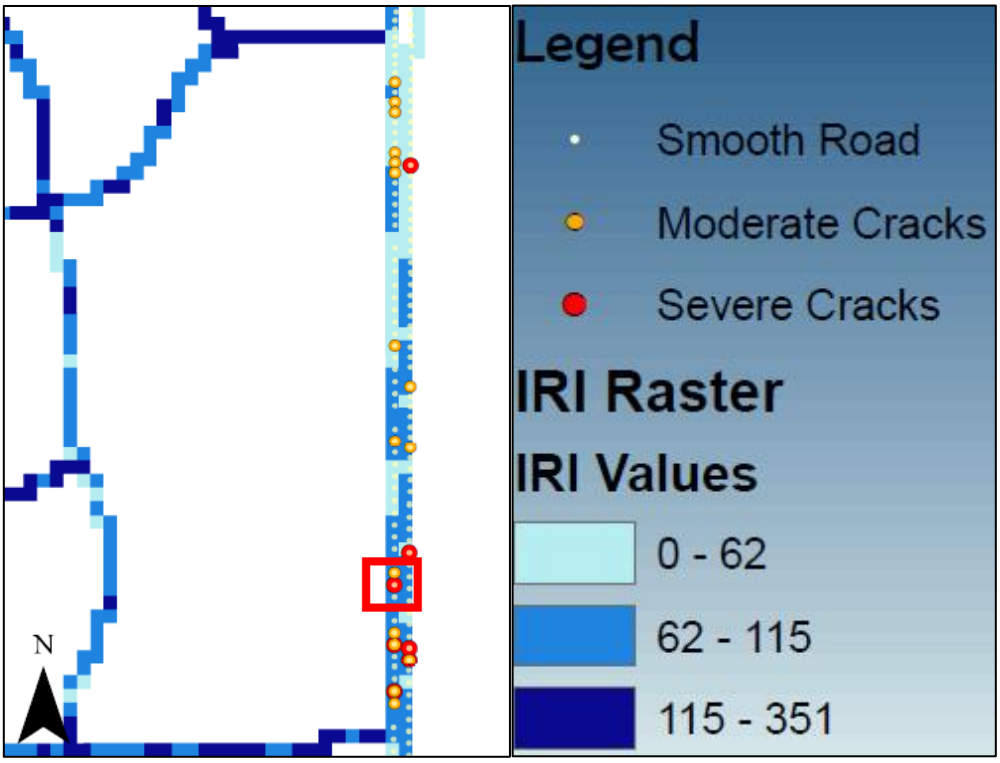

***Figure 33**: ADOT IRI values mapped with individual cracks located from the accelerometers.*

5.0 Analysis

After reviewing the results from the threshold method, average method, and GIS mapping, the team wanted to look more in-depth between the relationship between temperature and vibration. The following section looks at tire pressure effects, converting vehicle-based accelerometer data into IRI values and comparing them with ADOT's IRI values, and using statistical analysis.

5.1 Tire Pressure

It is known that tire pressure increases roughly 1-psi for every 10^{o}F. Throughout the year of data collection, the outside air temperature changed by about 80^{o}F from winter to summer. The question is whether an 8-psi difference effect the vibration during testing. A test was conducted that held tire pressure at 34-psi then more tests were conducted after holding the tire pressure to 44-psi. 44-psi was the maximum air pressure that the tire brand recommended. This procedure was conducted by filling and releasing air at the nearest gas station and using a tire pressure gauge to achieve the desired psi.

The following Figures 34 & 35 show how an increase of tire pressure does increase the vibration experienced by the vehicle. Therefore, in warmer temperatures, vehicle tires will impact pavement deficiencies at a harder rate and ware down the road faster than at cold temperatures. Controlling tire pressure during a road roughness test would be a challenging task. Tire pressure is constantly adapting to the outside temperature and road conditions. When a tire hits a crack, along with the built-up friction from the road, the tire pressure will fluctuate and stabilize quicker. If tire pressure is trying to be controlled, then the pressure

would have to be reset every couple of minutes which is not ideal from conducting a quick and easy test.

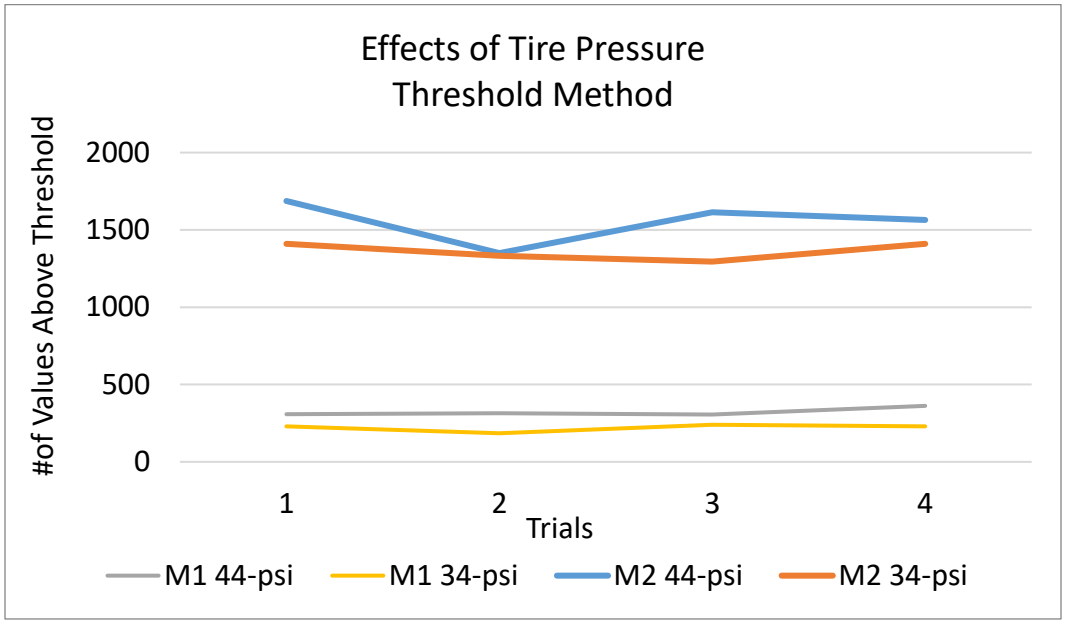

***Figure 34**: Threshold method - effects of tire pressure.*

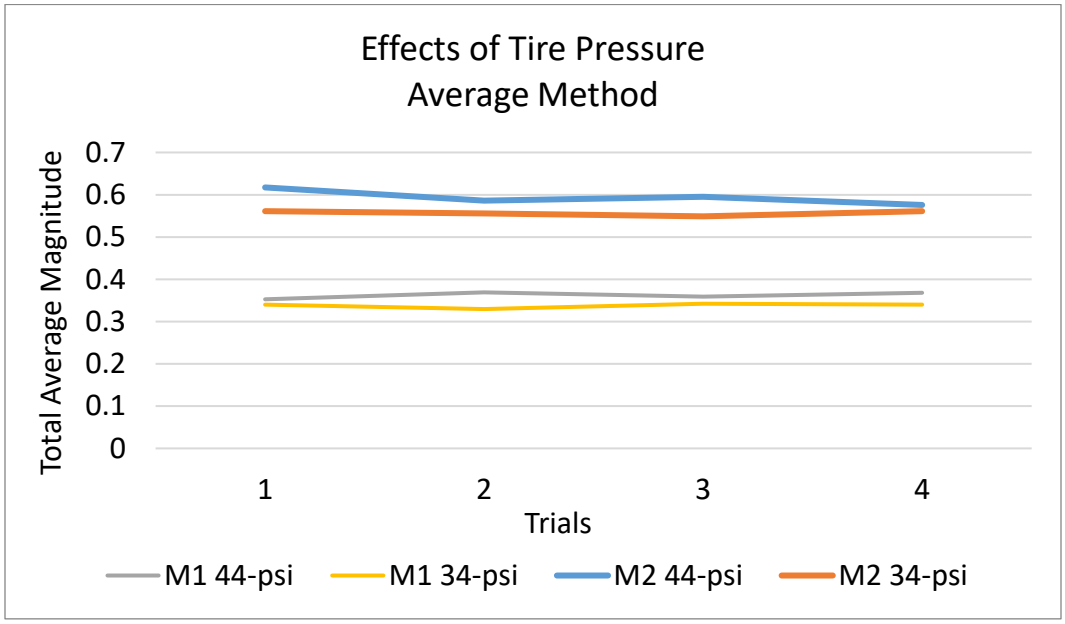

***Figure 35**: Average method - effects of tire pressure.*

5.2 IRI Conversion

IRI values are measurements of the averages of pavement distress over segments of road. ADOT provides IRI values in 0.1-mile segments. Therefore, one major crack in a segment of road can cause the IRI of that segment to appear rougher than it really is. This system differs by providing 0.1-mile segment IRI values as well as individual critical crack locations.

The national average of IRI thresholds provided by the Federal Highway Administration are as follows: less than 95-in/mi = good, 96-in/mi – 170-in/mi = acceptable, greater than 170-in/mi = bad. However, this is a comprehensive scale for all roads across the nation and may not be accurate for the general perception of road users in a certain region. These values do not reflect the perception of ride smoothness of motorists in a dense urban environment such as Phoenix [6]. States are now developing their maintenance strategies and IRI perception based on their personal needs. Based on recent data from Arizona's Highway Performance Monitoring System (HPMS), 86% of Arizona's urban Interstate lane miles have an IRI of 95 or better [18]. The test sections of this project are considered to have "good" IRI values. Based on ADOT's 2016 IRI data, the Baseline Rd. - Chandler Blvd. section is comfortably under the "good" threshold while 27th Ave. – 51st. Ave. is "good" but approaching the "fair" threshold as shown below.

Studies have shown [16], [19] that the power spectral density (PSD) method has a linear relationship with IRI. The PSD describes how the power of a signal is distributed over time and is usually used for random vibration analysis. The spectral content of the signal can be estimated when the PSD is taken as a mean squared magnitude, or a discrete Fourier transform (DFT), The equation is derived by using Laplace transforms.

$$IRI = C * \varphi_Z = C * \sqrt{\int_{-\infty}^{\infty} |H_{ZY}(\omega)|^2 \left(\frac{v}{\omega}\right)^4 S_a(\omega) d\omega}$$ Where,

φ_Z = mean square value of acceleration spectra

C = linear coefficient determined by field tests.

v = measuring speed.

ω = angular frequency.

$H_{ZY}(\omega)$ = frequency response function of $Z_s - Z_u$.

$S_a(\omega)$ = acceleration spectra.

To convert accelerometer data into IRI data, the DFT was performed in Microsoft Excel using an add-in called NumXl. The DFT function can be thought as a moving average of the vibration frequency and is shown in Figure 36. IRI values were converted by taking the average of the four sensors on each wheel. After the raw acceleration data was broken up into 0.1-mi segments, the amplitudes of the DFT function correspond to the averages of each 0.1-mile segment. The amplitudes of the moving average can be converted into IRI values. Each segment was converted to an IRI value and compared with ADOT IRI values from 2016, Figures 37 - 40.

The effects of pavement temperature earlier in this report were shown to hold weight in the observable vibration and therefore influence the IRI calculation. This report proposes that the equation be modified to account for temperature variation and the corresponding tire pressure variation.

$$IRI = C * \varphi_Z * (T_p * C_T)$$

DFT_x = discrete Fourier transform power signal at a certain segment, x.

T_P = pavement temperature.

C_T = linear coefficient of tire pressure determined by field tests.

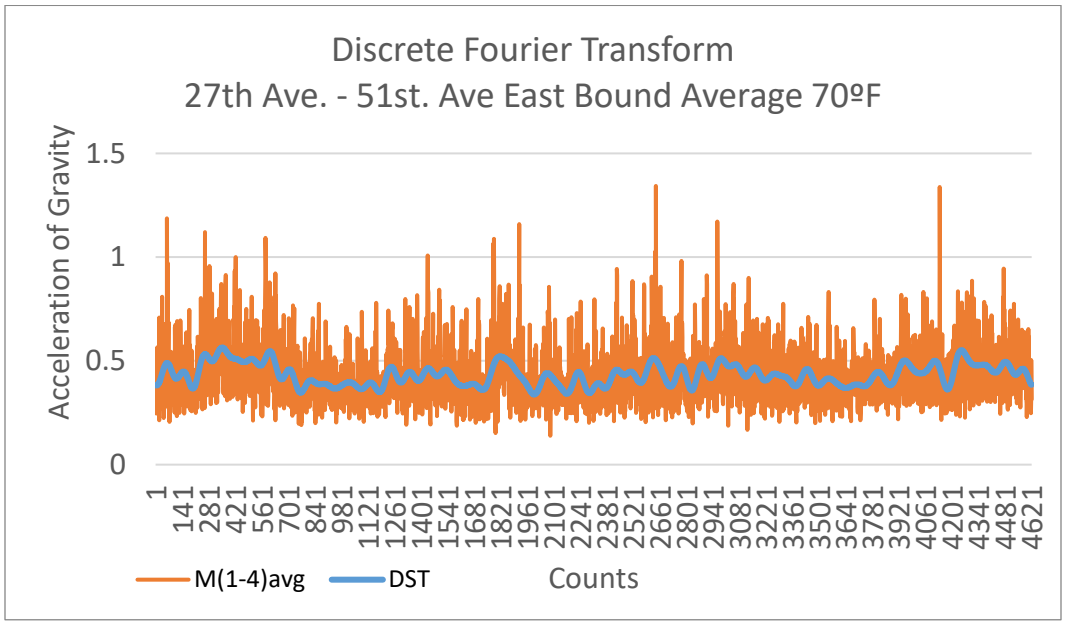

***Figure 36**: Discrete Fourier transform moving through raw data.*

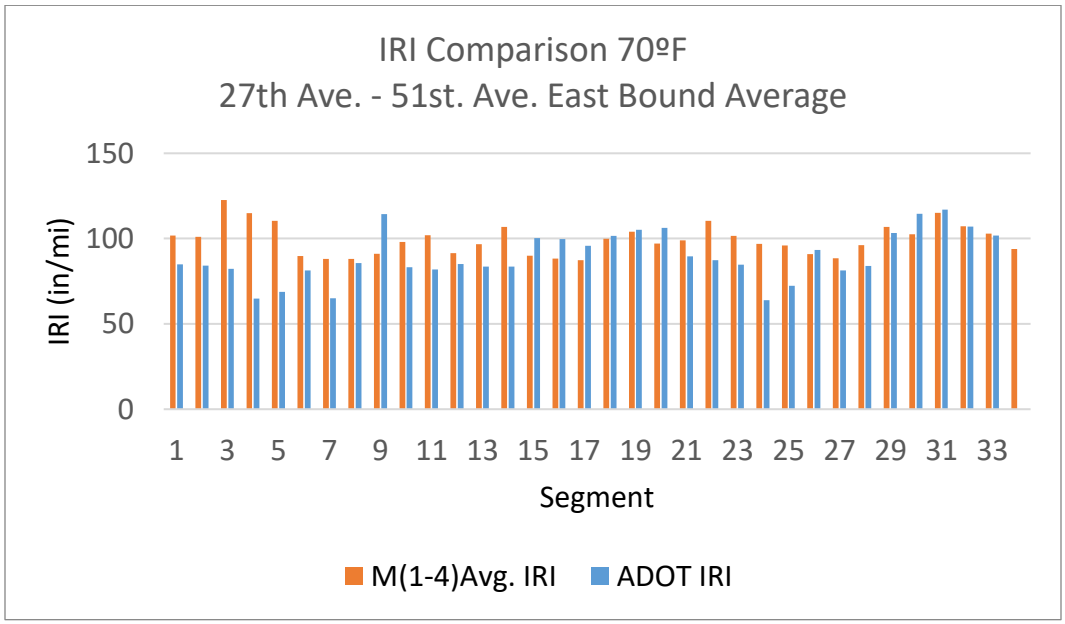

***Figure 37**: IRI comparison. 27th Ave. - 51st. Ave. east bound.*

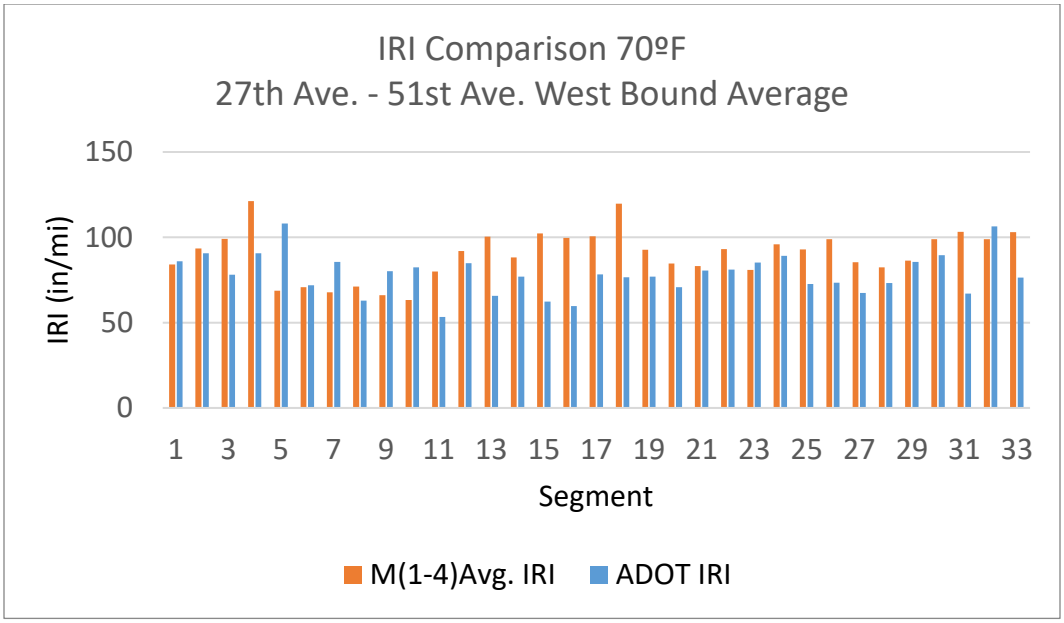

***Figure 38**: IRI comparison. 27th Ave. - 51st. Ave. west bound.*

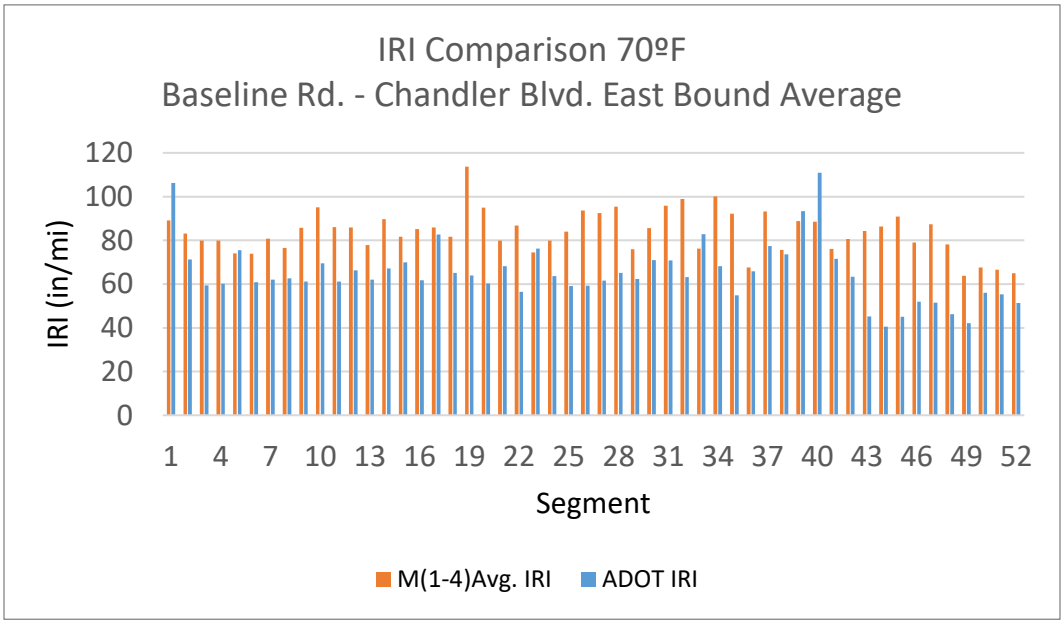

***Figure 39**: IRI comparison. Baseline Rd. - Chandler Blvd. east bound.*

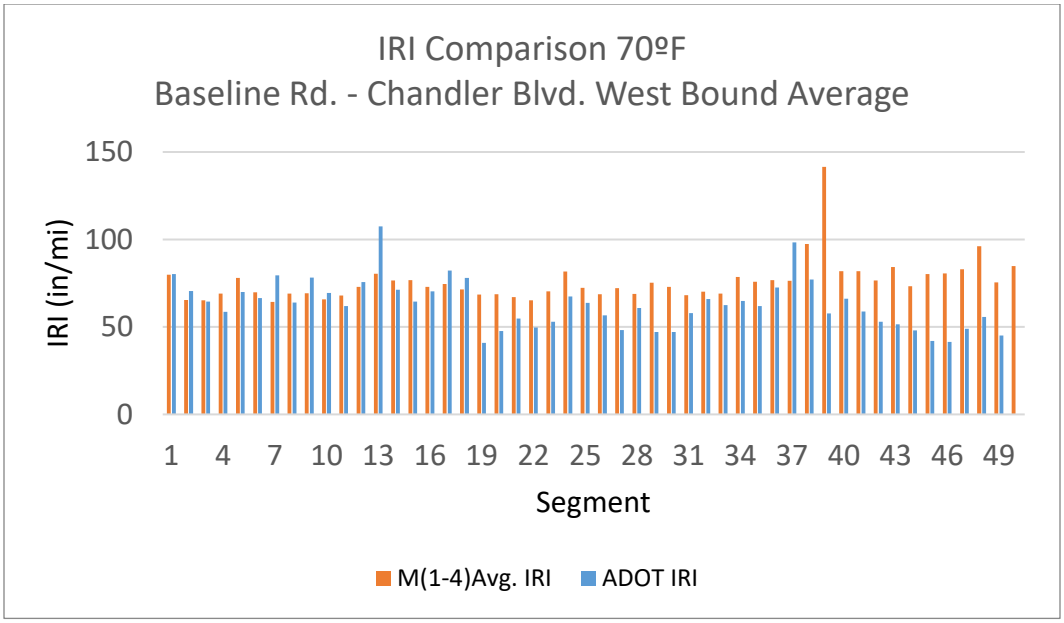

***Figure 40**: IRI comparison. Baseline Rd. - Chandler Blvd. west bound.*

5.3 Statistical Significance

The three types of statistical tests performed were T-tests, ANOVA, and Linear Regression using the statistical program jamovi. First, the team wanted to determine whether if vibration is dependent on temperature as noticed in the results using the threshold and average method above. The results indicated that both methods showed significant agreement that vibration changes with temperature with a p-value of less than 0.05. The Threshold method showed more significance having a higher F statistic but both methods were satisfactory in determine the relationship between temperature and vibration. The following ANOVA tests, Figures 41 & 42 show the threshold method followed by the average method.

ANOVA

ANOVA

	Sum of Squares	df	Mean Square	F	p
Temperature	1.02e+6	9	113858	14.9	< .001
Residuals	517946	68	7617		

***Figure 41**: ANOVA test. Threshold method. Temperature vs. vibration.*

ANOVA

ANOVA

	Sum of Squares	df	Mean Square	F	p
temp	0.341	9	0.03794	7.40	< .001
Residuals	0.359	70	0.00512		

***Figure 42**: ANOVA test. Average method. Temperature vs. vibration*

Next, the team wanted to know if the IRI data from ADOT matched the IRI data calculated from the accelerometers. This was done by using a paired sample T-test to compare the distribution of the two data sets. The results show that the distribution of the ADOT IRI is statistically similar to the distribution of the accelerometer IRI data having a p-value of less than 0.05. The following tests, Figures 43 – 46, are from the 27th Ave. – 51st Ave. East Bound Average, 27th Ave. – 51st Ave. West Bound Average, Baseline Rd. – Chandler Blvd. East Bound Average, and Baseline Rd. – Chandler Blvd. West Bound Average respectively.

Paired Samples T-Test

Paired Samples T-Test

			statistic	df	p
ADOT IRI	M(1-4)Avg. IRI	Student's t	−3.36	32.0	0.002

***Figure 43**: T-test IRI comparison. 27th Ave. - 51st. Ave. east bound.*

Paired Samples T-Test

Paired Samples T-Test

			statistic	df	p
ADOT IRI (2)	M(1-4)Avg. IRI (2)	Student's t	−3.51	32.0	0.001

***Figure 44**: T-test IRI comparison. 27th Ave. - 51st. Ave. west bound.*

Paired Samples T-Test

Paired Samples T-Test

			statistic	df	p
ADOT IRI (3)	M(1-4)Avg. IRI (3)	Student's t	−8.97	51.0	< .001

***Figure 45**: T-test IRI comparison. Baseline Rd. – Chandler Blvd. east bound.*

Paired Samples T-Test

Paired Samples T-Test

			statistic	df	p
ADOT IRI (4)	M(1-4)Avg. IRI (4)	Student's t	−4.91	48.0	< .001

***Figure 46**: T-test IRI comparison. Baseline Rd. – Chandler Blvd. west bound.*

The team hypothesized that the sensor inside the vehicle (M5) was sensing a function of the four sensors mounted on the wheels (M1-M4). To develop a model that could prove significance, linear regression was used, Figure 47. The equation would look like this:

$$M5 = \alpha_1 M1 + \alpha_2 M2 + \alpha_3 M3 + \alpha_4 M4 + \alpha_5$$

Linear Regression

Model Fit Measures

Model	R	R^2
1	0.715	0.511

Model Coefficients

Model	Predictor	Estimate	SE	t	p
1	Intercept	−0.2195	5.6919	−0.0386	0.969
	M1	−0.0416	0.0279	−1.4917	0.141
	M2	−0.1046	0.0445	−2.3530	0.022
	M3	0.1043	0.0190	5.4930	< .001
	M4	0.2358	0.0923	2.5543	0.013

***Figure 47**: Sensor M5 inside the vehicle is a linear function of all tires M1-M4.*

The R^2 value of 0.51 is not ideal but is still enough evidence to say the model exists. The negative values in the estimated alpha values are likely due to the orientation of M1 and M2 being in front of M5, on the front tires, while M3 and M4 are on the rear tires.

6.0 Conclusions:

This study shows that temperatures have a significant effect on vehicle-based accelerometer sensors. When comparing temperature to vibration, vibration increased as temperature increased in an exponential way. Tire pressure was proven to have a role in this relationship.

This report proposes that a temperature/tire pressure coefficient be applied to the IRI conversion formula.

It is shown that combining IRI datasets with severe and moderate crack locations, with pictures of the individual cracks, can be successful in providing a more precise evaluation of the road. As temperature is not usually considered a factor in determining IRI, this report proposes that highway agencies should pay more attention to which temperatures they are testing at with their instrumented vehicles.

The vehicle-based sensors were shown to have more consistency than smartphone sensors located inside the car. Limitations include orientation of the sensors. Using the method prosed in this project, the sensors were placed in the same project enclosures, same foam insulation, and same location every test run. However, exact placement could not be achieved for every road test. This should be perfected in the future for calibration consistency. Benefits of vehicle-based sensors over smart phone sensors include longer travel storage, more communication options, wider range of application, and deterioration detection of both sides of a lane.

Future work involves further testing to determine what degree accelerometer sensors are influenced by potential sources of error such as type of vehicle, variable speeds, wear of vehicle, wear of tires, tire pressure, suspension and dampening systems. The development of the proposed temperature coefficient could be determined by keeping track of tire life and mileage put on the vehicle. A constant vehicle with the same driver should be used for this as the vehicle used in this report was a NAU vehicle that was rented out every week to different drivers where unknown wear and tear was accumulated. Because crack classification varies

with temperature changes, a database of temperature coefficients would need to be created to determine how severe a crack is when detected under a given temperature.

6.1 Recommendations

The increased tire pressure resulting from the warmer temperatures will produce larger roughness values. It is recommended to not test during hot temperatures unless specifically looking for pavement distress due to temperature. Testing with vehicle-based accelerometers should be conducted at the average temperature that the region receives. It is not recommended to attempt to control tire pressure as the tire pressure will be constantly stabilizing throughout the test. Instead, a coefficient should be applied to account for pavement temperature and pavement temperatures should be measured frequently. It is unclear what temperatures current highway agencies test for IRI values or if tire pressures are controlled or accounted for. This report poses suspicion that profilers used by highway agencies could be affected by temperature and the resulting tire pressure differences. Pavement temperatures should be reported along with the IRI.

Tire pressure is the major contributing factor to increased vibration seen in this project. However, the nature of asphalt viscosity and the phenomenon of cracks and construction joints expanding and contracting throughout the day during different temperatures and loading could also be a contributing factor to the increased vibration seen in this experiment.

References

1. Arhin, S. A., Noel, E. C., and Ribbiso, A. “Acceptable International Roughness Index Thresholds based on Present Serviceability Rating,” Journal of Civil Engineering Research, Vol. 5 No. 4, pp. 90-96, 2015.
2. Buttlar, W.G., Islam, S. “Integration of Smart-Phone-Based Pavement Roughness Data Collection Tool with Asset Management System.” USDOT Region V Regional University Transportation Center Final Report, June 2014.
3. Douangphachanh, V.: Oneyama, H. “Using Smartphones to Estimate Road Pavement Condition.” International Symposium for Next Generation Infrastructure in Wollongong, Australia, October 1-4, 2013.
4. Du, Y., Liu, C., Wu, D., and Li, S. “Application of Vehicle Mounted Accelerometers to Measure Pavement Roughness.” International Journal of Distributed Sensor Networks, January 2016.
5. Du, Y., Liu, C., Wu, D., and Jiang, S. “Measurement of international roughness index by using Z-axis accelerometers and GPS,” Mathematical Problems in Engineering, vol. 2014, Article ID 928980, 10 pages, 2014.
6. Federal Highway Administration. “Pavement Smoothness Index Relationships: Final Report”. U.S. Department of Transportation. Turner-Fairbank Highway Research Center. 2002.
7. Gillespie, T.D., Sayers, M.W., and Segel, L. “Calibration of Response-Type Road Roughness Measuring Systems.” NCHRP Report. No. 228, December 1980.

8. Ho, C.H, Lai, C., and Almonnieay, A. “Using Geographic Information systems and Smartphone-Based Vibration Data to Support Decision Making on Pavement Rehabilitation.” Proceedings of the 2016 Information Processing and Management of Uncertainty (IPMU) Conference in Eindhoven, the Netherlands, June 20-24, 2016.
9. Kyriakou, C., Christodoulou, S. “Detecting Pavement Patches Utilizing Smartphones Technology and Vehicles.” Research Gate Conference in Heralion, Greece, July 2017.
10. Pantha, B. R., Yatabe, R. and Bhandary, N.P. GIS-Based Highway Maintenance Prioritization Model: an Integrated Approach for Highway Maintenance in Nepal Mountains. Journal of Transport Geography, vol. 18, pp. 426–433. 2010.
11. Pavementinteractive.org. Roughness | Pavement Interactive. Available at: http://www.pavementinteractive.org/roughness/. 2018.
12. Rodrigues, D. S., Ribeiro, P. J., and Nogueira, I. C. Safety Classification Using GIS in Decision-Making Process to Define Priority Road Interventions. Journal of Transport Geography, vol. 43, pp 101-110. February 2015.
13. Sayers, M.W., Gillespie, T. D., and Paterson, W. D. “Guidelines for the conduct and calibration of road roughness measurements,” World Bank Technical Paper 46, The World Bank, Washington, DC, USA, 1986
14. Sayers, M. W., Gillespie, T. D., and Queiroz, A. V. “The International Road Roughness Experiment. Establishing Correlation and a Calibration Standard for Measurements,” Tech. Rep. WTP45, 1986.
15. Sayers, M. W. “Two Quarter-Car Models for Defining Road Roughness: IRI and HRI.” Transportation Research Record 1215, pp. 165-172. 1989.

16. Sayers, M.W. and Karamihas, S.M., The Little Book of Profiling: Basic Information about Measuring and Interpreting Road Profiles, University of Michigan Transportation Research Institute., 1997.
17. Scavuzzo, R. W., Richards T. R., and Charek L. T. “Tire Vibration Modes and Effects on Vehicle Ride Quality”. Tire Science and Technology: January 1993, Vol. 21, No. 1, pp. 23-39. 1993.
18. What Moves You Arizona, “Final Working Paper #3. Existing Conditions, Deficiencies and Future Needs.” Arizona Long Range Transportation Plan Update. 2017
19. Zhou, X., Yan, L., and Sun, L. “Study and validation of the relationship between international roughness index and power spectral density,” China Civil Engineering Journal, vol. 40, no. 1, pp. 99–104, 2007.